ABSTRACT

RICCA, HENRY FRANCIS. Advances Towards Developing an Operational Model for Hydraulics and Water Quality in Water Distribution Systems. (Under the direction of Dr. Gnanamanikam Mahinthakumar).

This thesis presents a number of advances towards developing an operational model for water distribution systems. It focuses on two aspects: hydraulics and water quality. On the hydraulics side, procedures based on various types of data collected in water distribution systems are developed to reduce error in hydraulic models. On the water quality side, operational data and reaction kinetics are used to build a chloramine decay model in water distribution systems.

Reduction of error in water distribution network (WDN) models leads to simulations that are more representative of actual network conditions and allows for more effective experimentation and realistic system responses. Data collection in WDNs is becoming more prevalent as technological improvements allow data to be collected with increasing ease and quickness. This study quantifies the reduction in model error when considering demand uncertainty by incorporating pressure reducing valve (PRV) monitoring, operational monitoring, and supervisory control and data acquisition (SCADA) system data. PRV monitoring, operational monitoring, and SCADA data can be used together to model a sub-area of a full water distribution network and enforce observed head/flow conditions at the boundaries, observed total flow, and observed tank elevations and pump and valve controls. Forcing the head at the isolated section inflow boundaries and forcing the flow at the isolated section outflow boundaries with real field measurements reduces the model error due to demand and other network input uncertainties outside of the isolated section. Similarly, head boundary conditions can be fixed at all tanks by setting tank levels to the observed levels. Although there is uncertainty in individual demands, demand uncertainty can be reduced by matching the total

network flow. For this study, outputs obtained by the modeling software EPANET for a WDN model built with hourly measured demands were treated as actual network observations. Model error is determined by comparing the pressures obtained from models implementing PRV monitoring, operational monitoring, and SCADA data individually and in combination to pressures obtained from the model built with hourly measured demands. Results show that pressures simulated by the network model that incorporated PRV monitoring, operational monitoring, and SCADA data had less error than pressures simulated by a base model representative of what water managers would use without access to this data. Model improvement varies both spatially and temporally.

Chloramines are commonly used as secondary disinfectants in drinking water treatment, providing a residual for long lasting disinfection as drinking water moves through pipes to consumers. It is important for a desirable disinfection residual to be maintained throughout a distribution system to ensure that potentially harmful organisms present in the system are inactivated. Though chloramines are generally considered less reactive than free chlorine, they are inherently unstable, and undergo autodecomposition reactions even in the absence of reactive substances. In the presence of natural organic matter (NOM), chloramine loss is accelerated due to additional reaction pathways resulting in NOM oxidation. In this study, we have modeled chloramine loss due to autodecomposition and the presence of NOM in a batch system using MATLAB. The capabilities of the EPANET-MSX toolkit to model chloramine loss in a full scale water distribution network are also explored. A case study was carried out for the Town of Cary's water treatment facility and distribution network. First, a hydraulic model of Cary's water distribution system, which has about 27,000 nodes, was developed and calibrated using the EPANET toolkit with operational and water demand data supplied by Cary. Then water age

from the calibrated hydraulic model was used in conjunction with the batch model of chloramine decay to successfully predict chloramine concentrations spatially and temporally throughout the network.

Advances Towards Developing an Operational Model for Hydraulics and Water Quality in Water Distribution Systems

by
Henry Francis Ricca

A thesis submitted to the Graduate Faculty of
North Carolina State University
in partial fulfillment of the
requirements for the degree of
Master of Science

Environmental Engineering

Raleigh, North Carolina

2018

APPROVED BY:

_____	_____
Dr. Gnanamanikam Mahinthakumar Committee Chair	Dr. Emily Berglund
_____	
Dr. Detlef Knappe	

BIOGRAPHY

Henry Ricca was born in Durham, North Carolina on May 31, 1994 and raised in rural Rougemont, North Carolina. In Rougemont, he spent most of his childhood exploring the woods, splashing in the creek, listening to The Beatles, and playing baseball in the front yard with his little brother, Joey. In sixth grade he moved to Hillsborough, North Carolina, where he lived until he graduated from Orange High School in 2012. In his time at Orange High, he played baseball, ran cross-country, and fell in love with fishing and paddling on the Eno River.

After high school graduation, Henry attended North Carolina State University to study engineering. During his undergraduate years, he discovered his interest in understanding and improving human interactions with water. He obtained his Bachelor of Science in Environmental Engineering from NC State in 2016, and then continued his studies toward a Master of Science in Environmental Engineering at NC State. Water distribution system modeling was the main focus of his research. After completing his Master of Science, Henry will begin his professional career as a water engineer with Hazen and Sawyer in Raleigh, North Carolina.

ACKNOWLEDGMENTS

First, I would like to thank my advisor, Dr. Kumar Mahinthakumar, for the opportunity to work with him. His support and guidance were crucial to my navigation of the unknown waters of graduate school and his calm demeanor and patience kept me on track, even in stressful times. I would like to thank Drs. Berglund and Knappe for serving as committee members too. Further, I would like to express my gratitude to Dr. Jason Patskoski and Dr. Vasanthadevi Aravinthan for working so closely with me in the development of the papers presented in this thesis. Thank you both for investing so much of your time into making me a better researcher and a more curious, thoughtful person. In addition, I would like to thank my undergraduate advisor, Dr. Andrew Grieshop, for introducing me to the world of research and for his guidance and support of my future. I would also like to thank Dr. Jason Dorn for the invaluable experience I gained as an intern with his engineering firm. It was truly a privilege to work with and learn from all of you.

I also want to show my appreciation to the friends I met during my time at NC State. You were always there to celebrate with me in the good times and keep my head straight during the rough, stressful times. I hope I can repay you in the same fashion.

Finally, I would like to give my most sincere thanks to my parents, Jean and Dan, and my brother, Joe. I certainly would not be where I am today without your support, encouragement, and unconditional love. I can't believe how lucky I am to have you. I love you.

TABLE OF CONTENTS

LIST OF TABLES

LIST OF FIGURES

INTRODUCTION

This thesis is organized as two papers in journal format. The first paper, presented in chapter 1, focuses on utilizing data that can be collected in water distribution networks to reduce network model error due to demand uncertainty, and quantifying the reduction in model error. In this paper we use the EPANET modeling toolkit and focus on four types of data that can be collected in water distribution systems – pressure reducing valve (PRV) monitoring data, operational monitoring data, supervisory control and data acquisition (SCADA) system data, and advanced metering infrastructure (AMI) system data. The reduction in model pressure error that can achieved by incorporating PRV monitoring data, operational monitoring data, and SCADA system data is quantified. Since no measured pressure data was available for this study, the outputs from a model built with AMI data were treated as measured values. This study employed models and data from the Town of Cary's water distribution network. Results show that incorporating PRV monitoring, operational monitoring, and SCADA system data together reduces hydraulic model error and that the reduction in model error varies spatially and temporally.

The second paper, presented in chapter 2, focuses on modeling chloramine decay in full scale drinking water supply systems. Chloramine is a commonly used secondary disinfectant which undergoes decay due to autodecomposition reactions and the oxidation of natural organic matter that is present in the water. For this paper, a batch model of chloramine decay is used along with water age to predict chloramine concentrations spatially and temporally throughout a water distribution network. A case study was carried out to the Town of Cary's water distribution network, and a hydraulic model was developed and calibrated using the EPANET toolkit and operational and water demand data supplied by Cary. Water age was extracted from

this calibrated hydraulic model, and concentrations predicted by the model were compared to disinfectant concentrations measured in Cary's system. The capabilities of the EPANET-MSX toolkit to model chloramine loss in a full scale water distribution network are also explored.

CHAPTER 1

Reducing Error in Water Distribution Network Simulations through Boundary Condition Forcings using Field Measurements

Abstract

Reduction of error in water distribution network (WDN) models leads to simulations that are more representative of actual network conditions and allows for more effective experimentation and realistic system responses. Data collection in WDNs is becoming more prevalent as technological improvements allow data to be collected with increasing ease and quickness. This study quantifies the reduction in model error when considering demand uncertainty by incorporating pressure reducing valve (PRV) monitoring, operational monitoring, and supervisory control and data acquisition (SCADA) system data. PRV monitoring, operational monitoring, and SCADA data can be used together to model a sub-area of a full water distribution network and enforce observed head/flow conditions at the boundaries, observed total flow, and observed tank elevations and pump and valve controls. A model isolation procedure was developed to model sub-areas of a network. Forcing the head at the sub-area inflow boundaries and forcing the flow at the sub-area outflow boundaries with real field measurements reduces the model error due to demand and other network input uncertainties outside of the isolated section. Similarly, head boundary conditions can be fixed at all tanks by setting tank levels to the observed levels. Although there is uncertainty in individual demands, demand uncertainty can be reduced by matching the total network flow. For this study, outputs obtained by the modeling software EPANET for a WDN model built with hourly measured demands were treated as actual network observations. Model error is determined by comparing the pressures obtained from models implementing PRV monitoring, operational monitoring, and SCADA data

individually and in combination to pressures obtained from the model built with hourly measured demands. Results show that pressures simulated by the network model that incorporated PRV monitoring, operational monitoring, and SCADA data had less error than pressures simulated by a base model representative of what water managers would use without access to this data. Model improvement varies both spatially and temporally. Models with reduced error can aid water utility managers in decision making related to daily planning and operations, emergency response, energy management, and network repair scheduling, and also improve leak detection and planning for future network expansions and demand increases.

1.1 Introduction

Water distribution networks are the series of pipes, tanks, reservoirs, pumps, and valves that are responsible for conveying drinking water to homes, businesses, recreation areas, and agriculture. Understanding the intricacies of these networks can lead to a more efficient distribution of water, saving money and energy and improving the quality of the water. Modeling these networks plays a key role in understanding how the networks behave under different conditions, because conditions can be changed much more quickly and easily in models than they can in actual physical distribution systems. Further, the system response observations can be more frequent and denser in a model than the real system. With the use of models, the impact of leaks or pipe breaks in networks can be analyzed without actually disrupting the current operating conditions. There are several different software options that can be used to model water distribution systems including EPANET (2008), WaterCAD (2017), H2ONET (2018), and WaterGEMS (2017). This study was performed using EPANET, an open source demand driven modeling software. The term “demand driven” indicates that the demands in the model will always be met, regardless of the pressure in the network, as opposed to pressure driven models that use pressure as a

constraint, even if the pressure in the network keeps demands from being met. There is an extension available to make EPANET pressure driven, called EPANET-PDX (Siew and Tanyimboh, 2012).

Modeling water distribution networks is crucial to conducting quick and inexpensive experiments, but the models are only as accurate as the information used to build them. This poses a challenge for matching real water distribution system conditions with models because every source of data from distribution networks that is inputted to the software has uncertainty associated with it.

For instance, demands are typically measured once a month in the real systems, as part of monthly billing. These observations are then used to create demands at hourly time steps in models using typical demand patterns based on the water use (residential, industrial, etc.). While this process does give some insight into the behavior of the node, there is an extreme amount of uncertainty in the demands, especially at smaller time scales. Since EPANET is a demand driven software, every calculation performed by the software is based on the inputted demands. The high level of uncertainty associated with the demands makes accurately modeling distribution systems difficult, especially at smaller time scales.

The main source of head loss in water distribution systems is from pipe-wall friction due to pipe roughness. These pipe roughness coefficients are inputs to distribution models and are another source of uncertainty. Pipe roughness is based on the pipe material, but as pipes age they become rougher, increasing friction losses. The level of roughness can be estimated by pipe material and age, but there is a high level of uncertainty associated with this too. Pipe roughness changes at different rates depending on water quality and overall use, so predicting roughness years after pipes have been installed is difficult. Further, no pipe will age the same as another, so

determining the roughness coefficient for each pipe in the system is arduous. Since pipe roughness corresponds to head loss, the uncertainty in roughness results in uncertainty in head at each node, which compounds as pipes link together throughout the network.

The elevations of network nodes are also uncertain unless the depth of every node under the ground surface has been surveyed. This is highly unlikely, since every pipe intersection is a node and there are thousands of nodes in most water distribution networks. Further, most distribution systems were installed a long time ago, when surveying technology was not as accurate and precise as it is today. For modeling purposes, node elevations are most likely assumed to be a set distance beneath ground level using LIDAR, which also has a high level of uncertainty ("Light Detection and Ranging", 2015). A wide assumption like this leads to uncertainty since each node is likely not the exact same depth under the ground surface due to varying soil conditions and the presence of other pipes and wires running under the ground. This uncertainty in elevation relates to uncertainty in pressure at each node because elevation and pressure are directly related. One foot of difference in elevation corresponds to about 0.4 pounds per square inch (psi) of difference in pressure, so if elevation is not accurately represented in the model, pressure will not be accurately represented either.

Another source of uncertainty in water distribution networks is the presence of background leaks - small leaks from fittings in the network. These slight leaks are common in distribution networks, but are difficult to locate and quantify due to the relatively small leak quantity and the amount in the system. The only indication of their presence is a discrepancy between the amount of water leaving the water treatment plant and the amount of water that is metered and billed for. This discrepancy is usually resolved by dividing the extra demand evenly between the demand nodes in the network. However, this assumption is likely not accurate

because the background leaks occur at specific points in the network, not evenly throughout it. Further, background leaks are more prevalent in older pipes, which goes against the assumption that leaks are evenly distributed. These leaks increase flow in the network, which in turn lowers the pressure at each node. While distributing addresses the water quantity, the locations of these leaks are most likely not evenly distributed. Modeling based on this inaccurate demand assumption increases uncertainty in the model, specifically the pipe flow and node pressure.

While these uncertainties are in model input, other sources of uncertainty are due to how the network is managed and operated. For example, tank levels depend on when pumps are turned on and off and valves are opened and closed. Most pump and valve operations are controlled by humans, and can vary day by day based on the operator's discretion. For example, an operator may be busy doing other tasks and not be able to activate the pump at an exact instant. These day by day variations can't be easily modeled, adding further uncertainty to distribution network models. This uncertainty can be reduced by modeling fewer network components that rely on human controls.

All of these uncertainties compiled over an entire distribution network make it challenging to produce a water distribution model that accurately reflects real system conditions. However, improved technology has made data collection from water distribution systems more prevalent in recent years. Pressure and flow meters allow water utilities to measure pressure and flow at chosen points throughout the system. Supervisory control and data acquisition (SCADA) systems allow for the remote measurement, logging, and processing of data including tank level, pump and valve operation, pressure, and flow at defined time steps. Advanced metering infrastructure (AMI) systems can take water meter readings remotely at defined time steps.

The data collected with this equipment can be incorporated in water distribution network models to help the models more accurately reflect real system conditions. In this work, we employ four types of data with various spatial and temporal scales that may be collected in water distribution systems. The first type of data is pressure reducing valve (PRV) monitoring data, which is considered to be hourly hydraulic head measurements at system PRVs carrying flow into the section of interest and hourly flow measurements at system PRVs carrying flow out of the section of interest. PRVs are generally located at boundary points that separate hydraulic regions known as pressure zones. The second type of data is operational monitoring data, which is considered to be daily volumetric water treatment (WTP) plant output and start-of-day and end-of-day tank levels. The third type of data is SCADA data, which is considered to be hourly tank levels and continuous valve and pump conditions (either on or off). The model improvement resulting from employing these three types of data individually and in combination is quantified. The fourth type of data is AMI data, which is considered to be hourly demand measurements at all demand nodes. This data is used to create an ideal model representative of the real system. The outputs from this "real system" model are treated like actual field measured values and are used as a point of reference to quantify model error.

The goals of this study are to 1) develop procedures to incorporate PRV monitoring data, operational monitoring data, and SCADA system data into hydraulic models 2) quantify the reduction in model error due to demand uncertainty resulting from the incorporation of these types of data into models and 3) explore the spatial and temporal trends in the resulting model improvement.

1.2 Data

The Town of Cary's water distribution system, shown in Figure 1.1, was chosen as the basis of this experiment. The EPANET model of the Town of Cary's distribution network that was used as the base model for this study was developed by the private contracting company CH2M HILL for the Town of Cary (CH2M HILL, 2009). This model is skeletonized to 6 inch diameter pipes and demands are aggregated, meaning that no pipes smaller than 6 inches in diameter are shown in the network and the demands of pipes smaller than 6 inches are added to nodes on 6 inch or bigger pipes at the points in the network where the smaller pipes offshoot.

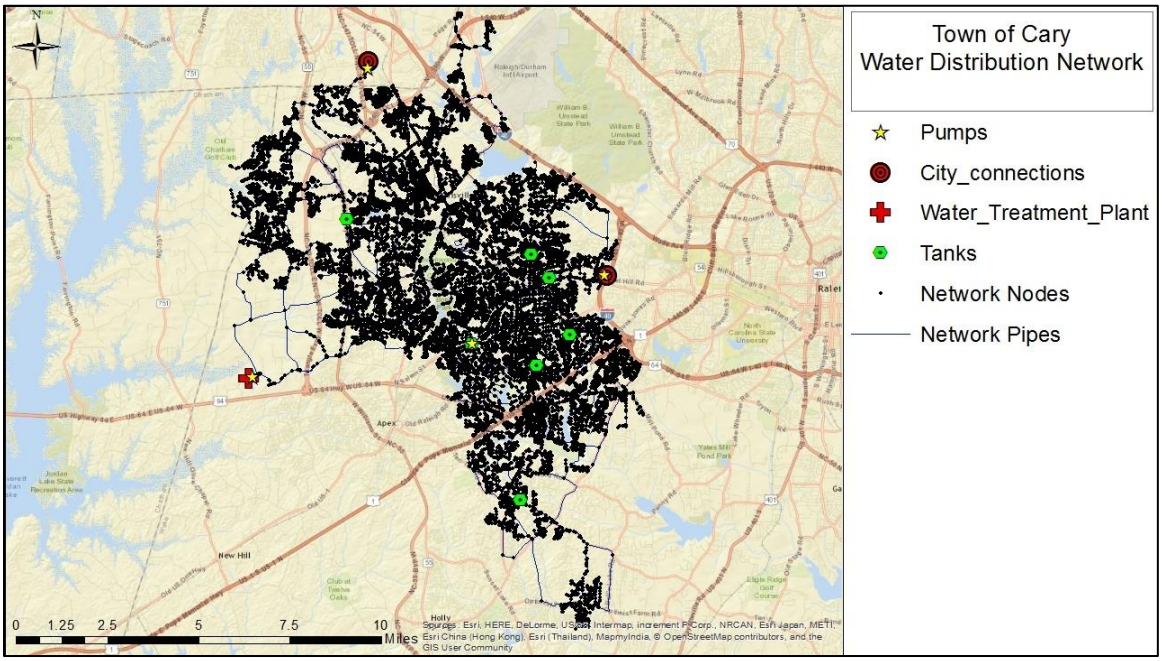

Figure 1.1. Town of Cary's water distribution network.

The network consists of 26986 total nodes (black circles in Figure 1.1), a water treatment plant that is modeled as a reservoir (cross shape in Figure 1.1), two city connections modeled as reservoirs (bullseyes in Figure 1.1), seven tanks (hexagons in Figure 1.1), 28331 pipes (black lines in Figure 1.1), twenty pumps (stars in Figure 1.1), and eleven valves (not shown in Figure 1.1). There are three pressure zones in the Town of Cary network that are divided based on ranges of pressure – the western, central, and southern pressure zones (not shown in Figure 1.1).

The main source of water for the Town of Cary network is the Cary/Apex Water Treatment Plant, which treats water from Jordan Lake and also supplies water to the Town of Apex, not modeled in this study. This treatment facility currently has a capacity of 40 million gallons per day. Pump stations supply water from the treatment plant to the central and western pressure zones, and the southern pressure zone is fed by the central pressure zone. During emergency situations, planned treatment plant shutdowns, or times of water scarcity, the Town of Cary network can draw water from the City of Durham and the City of Raleigh water distribution networks (city connections in Figure 1.1). These connections are represented with reservoirs in the EPANET model.

Of the seven tanks in the network, six are elevated tanks and one is a ground storage tank. The Carpenter Tank is the only tank in the western pressure zone and it has a usable volume of 2 million gallons. The central pressure zone has five tanks – the Ridgeview Tank, Maynard Tank, Harrison Tank, Field Street Tank, and Old Apex Tank. The Old Apex Tank is the network's lone ground storage tank, and it has a usable volume of 1.75 million gallons. The Ridgeview, Harrison, Field Street, and Maynard Tanks have usable volumes of 1 million gallons, 1 million gallons, 0.75 million gallons, and 0.5 million gallons respectively. The southern pressure zone has the Plumtree Tank, which contains a usable volume of 1 million gallons.

The twenty pumps in the Town of Cary network are split between a high speed pump station at the Cary/Apex water treatment plant and four booster pump stations spread throughout the network. The high speed pumping station at the treatment plant drives flow to the central and western pressure zones. The booster pump stations are used to convey water from ground storage tanks and from areas of low pressure to areas of high pressure. Three of the booster

pump stations in the network are only used in emergency situations and the fourth booster pump station is used to drive flow from the Old Apex ground storage tank.

The control valves in the network are used to control flow and pressure between pressure zones. Control valves are located between the central and western pressure zones and the central and southern pressure zones.

Pipe diameters in the network range from 42 down to 6 inches. Any existing pipes less than 6 inches in diameter are not shown in the model; their demands are accounted for in nodes on pipes that are 6 inches or bigger. About 62 percent of the pipes in the network are made of ductile iron, 23 percent of the pipes are made of asbestos cement, and about 13 percent of the pipes are made of PVC (CH2M HILL, 2009).

There is a wide range of data that may be collected from water distribution systems. The Town of Cary has invested in a SCADA system to remotely measure pressure and flow at key points in the network, tank levels, and pump and valve operations at hourly time steps. Cary has also invested in an AMI system to take hourly water meters readings remotely. Close to 60,000 AMI water meters have been installed in Cary's water distribution system. This represents a large investment in water distribution system data collection. Since Cary has the ability to measure hourly demands using their AMI system, they are capable of building models with practically no demand uncertainty. The results of this study can aid municipalities that have not already made large investments in water distribution system data collection in deciding which types of data collection to invest in for model improvement purposes.

The four types of data that this project focuses on are PRV monitoring data, operational monitoring data, SCADA data at tanks, pumps, and valves, and AMI data, as described in Figure 1.2. A model built with AMI data is considered to be representative of the real system in this

study. The model improvement resulting from employing PRV monitoring data, operational monitoring data, and SCADA data is quantified. These four types of data are collected at various spatial and temporal scales, as shown in Figure 1.3, and require different levels of monetary investment to collect. Generally, data collected at denser spatial and temporal scales is more costly to collect.

Monitoring Data Type	PRV monitoring	Operational monitoring	SCADA at tanks, pumps, & valves	AMI data
Observations	Hourly PRV hydraulic head for inflow, hourly PRV flow for outflow	Daily WTP output, daily tank levels	Hourly tank levels, continuous valve and pump conditions (on/off)	Hourly nodal demands

Figure 1.2. Descriptions of the monitoring data considered for this study.

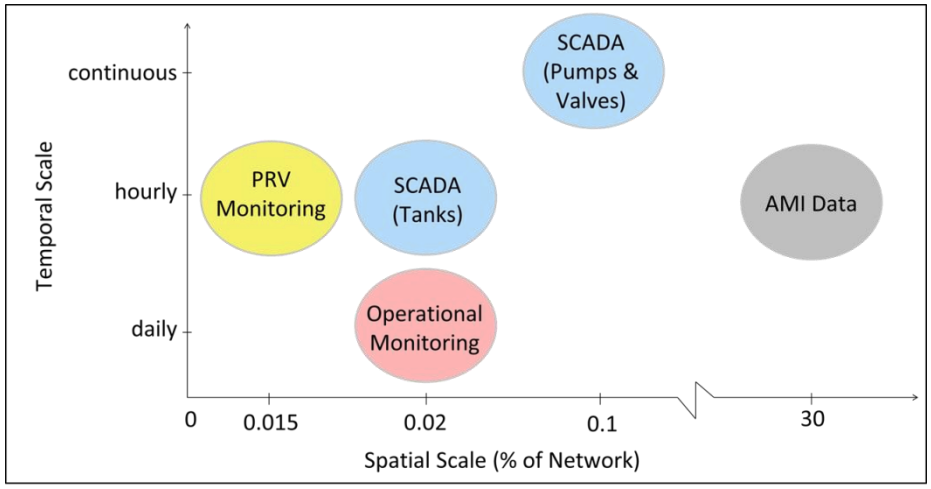

Figure 1.3. Spatial and temporal scales of monitoring data collected. Data collected at more dense spatial and temporal scales is more costly to collect.

1.3 Methods

The proposed model implementation of each data type discussed in section 1.2 is described simply in Figure 1.4. A thorough description of the process followed to implement each data type is presented in Figure 1.5.

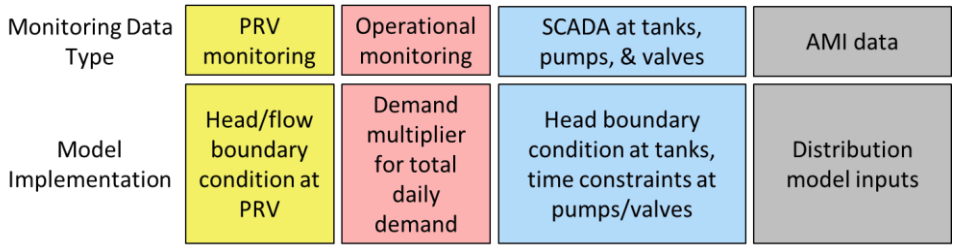

Figure 1.4. Proposed model implementation of monitoring data considered for this study.

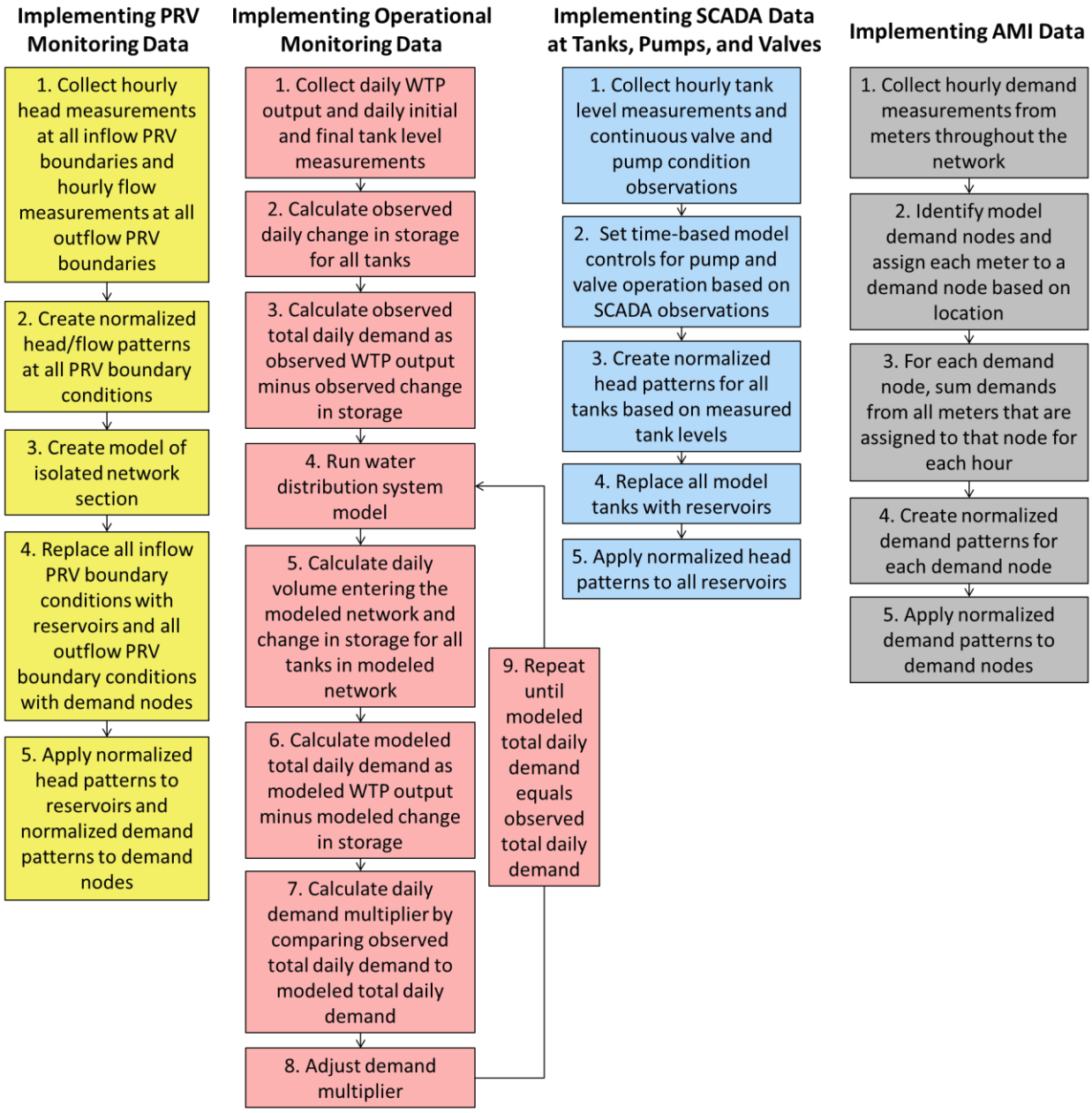

Figure 1.5. Model implementation process for PRV monitoring data, operational monitoring data, SCADA data at tanks, pumps, and valves, and AMI data.

PRV monitoring data can be implemented in water distribution system models for projects concerned with sub-areas of a network. A sub-model containing the section of interest can be created for any section of the network that can be completely isolated by making cuts at the PRVs, usually a network pressure zone. This isolated area should contain all of the nodes and pipes that are relevant to the experiment being conducted. PRVs at the boundary between the isolated section and the rest of the network must be cut in the model to isolate the desired area. PRVs that carry flow into or out of the isolated section must be modeled with boundary conditions when they are cut. Since adding boundary conditions increases the required observations in the real water distribution system, the section to be isolated should be chosen strategically to reduce the number of PRVs that need to be cut. Since EPANET is a demand driven modeling software, pressure cannot be directly input at nodes. This model isolation procedure circumvents this limitation.

To model severed PRVs that carry flow into the isolated section of the network, reservoirs must be placed at the locations of the PRV cuts in the isolated network. Since the pressure at the boundary needs to be considered in addition to the flow for water entering the isolated section, the total head of the added reservoir must match the total head in the original PRV at the boundary. To achieve this, head patterns must be created and applied to the added reservoirs. To model severed PRVs that carry flow out of the isolated section of the network, demand nodes must be placed at the locations of the PRV cuts in the network. Since only flow needs to be considered for water leaving the isolated section, the demand of the added demands node must match the flow of water leaving the isolated section in the original PRV at the boundary. To achieve this, demand patterns must be created and applied to the added demand nodes. These head and demand patterns can be at any desired time step so long as observations

in the field can be made at the same time step. When a live PRV carrying flow into or out of the network is cut, the following steps should be taken to model the boundary condition.

1. Collect hourly head measurements at each PRV carrying flow into the isolated section that must be cut to completely isolate the section of interest. Collect hourly flow measurements at each PRV carrying flow out of the isolated section that must be cut to completely isolate the section of interest. This is shown as step 1 in the "Implementing PRV Monitoring Data" section of Figure 1.5.
2. Normalize the head or flow at each hour by dividing the head or flow at each hour by a fixed value. This can be the average head/flow, maximum head/flow, or any other fixed value of head/flow. This is shown as step 2 in the "Implementing PRV Monitoring Data" section of Figure 1.5.
3. Create a model of the desired isolated section by removing all model components outside of the section from the original model. This is shown as step 3 in the "Implementing PRV Monitoring Data" section of Figure 1.5.
4. In the model, replace each PRV that has been cut at an inflow boundary of the isolated section with a reservoir. Replace each PRV that has been cut at an outflow boundary of the isolated section with a demand node. This is shown as step 4 in the "Implementing PRV Monitoring" section of Figure 1.5.
5. Set the total head of each reservoir added to the model to the value of head that was used to normalize the head at each hour and apply an hourly head pattern using the normalized heads calculated in step 2. Now the head at the inflow boundaries of the model of the isolated section should be equal to the head at the PRV in the actual network for each hour. Set the total demand of each demand node added to the model to the value of flow

that was used to normalize the flow at each hour and apply an hourly demand pattern using the normalized flows calculated in step 2. Now the flow at the outflow boundaries of the model of the isolated section should be equal to the flow at the PRV in the actual network for each hour. This is shown as step 5 in the "Implementing PRV Monitoring Data" section of Figure 1.5.

Forcing the head at the isolated section inflow boundaries and forcing the flow at the isolated section outflow boundaries with real field measurements reduces the model error due to demand and other network input uncertainties outside of the isolated section, while maintaining the signal from the rest of the network. For this study with the Town of Cary's water distribution network, the western pressure zone (WPZ) is isolated by making cuts at 26 pipes that carry no flow and 1 PRV that carries flow into the WPZ, as shown in Figure 1.6. Cutting the pipes that carry no flow doesn't affect conditions within the isolated section of the network and no boundary conditions are required. The inflow boundary condition at the PRV is modeled with a reservoir and head pattern as described above, with the hourly PRV head measurements taken from the outputs of the "real system" model.

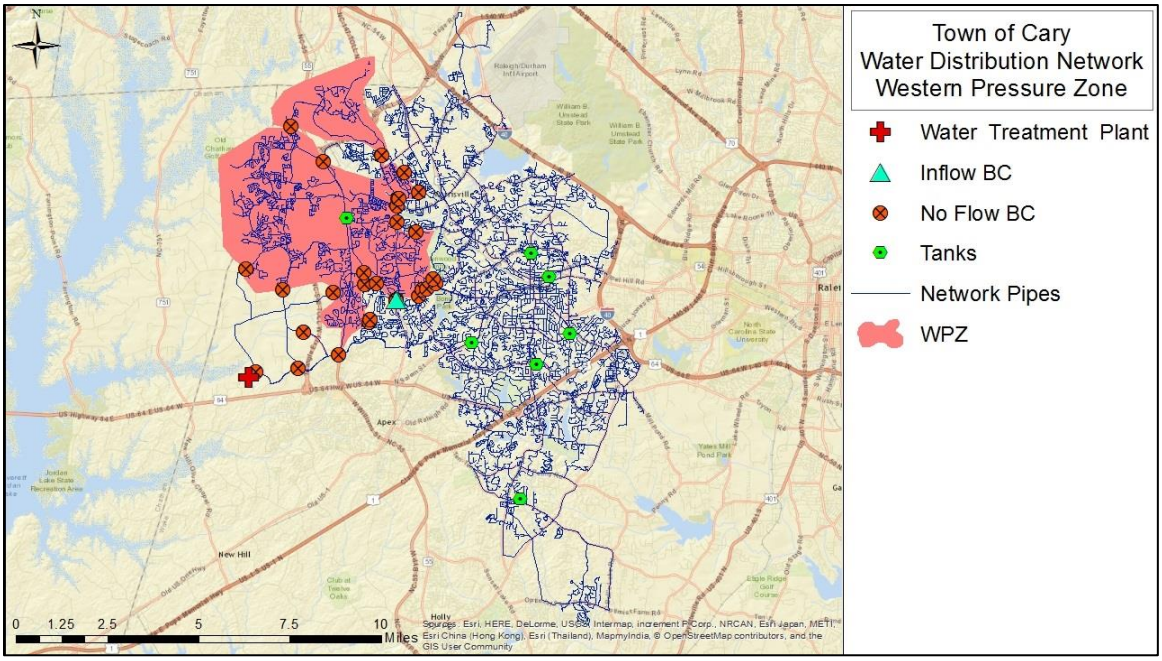

Figure 1.6. Pipe cuts made to isolate the WPZ of the Town of Cary's water distribution network. The WPZ is highlighted in red and all pipe cuts made to isolate the WPZ are shown. Cutting pipes that carry no flow doesn't affect conditions within the isolated section. The PRV that carried flow into the WPZ was modeled as an inflow boundary condition (BC) with a reservoir and head pattern.

Operational monitoring data can be used to match modeled total daily demand to observed total daily demand, assuming a model of the water distribution system of interest is available. This is achieved by applying a demand multiplier to the model. The total daily demand of the real system can be calculated from observed daily WTP output and observed daily initial and final tank levels at all network tanks. The demand multiplier to be applied to the model can be calculated by comparing this observed total daily demand to the modeled total daily demand. A new demand multiplier can be employed in the model for each day to reflect daily system demand variations. When operational monitoring data is available, the following steps should be taken to match total model demand to total observed demand.

1. Collect daily volume of water output by the WTP and daily initial and final tank level measurements for each tank. This is shown as step 1 in the "Implementing Operational Monitoring Data" section of Figure 1.5.

2. Use the daily initial and final tank level measurements to calculate the observed daily change in storage for all tanks in the network. The volume held in each tank is a function of the tank level, and change in storage is calculated as final volume held minus initial volume held. Final tank levels being higher than initial tank levels indicates a positive change in storage and initial levels being higher than final levels indicates a negative change in storage. The total change in storage for the network is the sum of the individual changes in storage from each tank. This is shown as step 2 in the "Implementing Operational Monitoring Data" section of Figure 1.5.
3. Use the observed daily volume of water output by the WTP and observed daily total change in storage to calculate the observed total daily demand. Observed total daily demand is calculated as observed daily WTP output minus observed daily total change is storage. This is shown as step 3 in the "Implementing Operational Monitoring Data" section of Figure 1.5.
4. Run the model of the water distribution system of interest. This is shown as step 4 in the "Implementing Operational Monitoring Data" section of Figure 1.5.
5. Use the model outputs to calculate the modeled daily volume of water output by the WTP and modeled daily change in storage for all tanks. The modeled total change in storage is the sum of the individual changes in storage from each modeled tank. This is shown as step 5 in the "Implementing Operational Monitoring Data" section of Figure 1.5.
6. Use the modeled daily volume of water output by the WTP and modeled daily total change in storage to calculate the modeled total daily demand. Modeled total daily demand is calculated as modeled daily WTP output minus modeled daily total change in

storage. This is shown as step 6 in the "Implementing Operational Monitoring Data" section of Figure 1.5.

7. Calculate a daily demand multiplier by comparing observed total daily demand to modeled total daily demand. The initial daily demand multiplier should be calculated by dividing observed total daily demand by modeled total daily demand. This is shown as step 7 in the "Implementing Operational Monitoring Data" section of Figure 1.5.
8. Adjust the model demand multiplier to match the calculated daily demand multiplier and re-run the model. Check if modeled total daily demand is equal to observed total daily demand. This is shown as step 8 in the "Implementing Operational Monitoring Data" section of Figure 1.5.
9. If modeled total daily demand equals observed total daily demand, stop. If not, repeat steps 4 – 8 until modeled total daily demand equals observed total daily demand. This is shown as step 9 in the "Implementing Operational Monitoring Data" section of Figure 1.5.

Although there will be uncertainty in individual model demands without the availability of hourly demand data, demand uncertainty can be reduced by matching the total network flow. For this study, the observed flow from the WTP and the observed beginning and end of day tank levels were taken from the outputs of the "real system" model and the demand multiplier was applied to the base model. This scaled the total demand in the base model up or down accordingly to match the "real system" total demand.

SCADA data at tanks, pumps, and valves can be used to match model pump and valve operations to observed pump and valve operations and create head boundary conditions at tanks. Matching observed pump and valve operations is achieved by setting time-based controls for

model pump and valve operations. Creating head boundary conditions at tanks is achieved by replacing model tanks with reservoirs and creating and applying head patterns to each reservoir. These head patterns can be at any desired time step so long as observations in the field can be made at the same time step. When SCADA data is available at tanks, pumps, and valves, the following steps should be taken to implement the data in a water distribution system model.

1. Collect hourly tank level measurements and continuous pump and valve condition (on/off, open/closed) observations. This is shown as step 1 in the "Implementing SCADA Data at Tanks, Pumps, and Valves" section of Figure 1.5.
2. Set time based model controls for pump and valve operation based on the SCADA observations. For example, if the SCADA system reports a valve closing at a specific time, a model control can be set to close the corresponding valve in the model at the same time. This is shown as step 2 in the "Implementing SCADA Data at Tanks, Pumps, and Valves" section of Figure 1.5.
3. Use the observed hourly tank levels to normalize the head at each tank at each hour by dividing the head at each hour by a fixed value. This can be the average head, maximum head, or any other fixed value of head. Tank head is equivalent to the bottom of tank bowl elevation plus tank level. This is shown as step 3 in the "Implementing SCADA Data at Tanks, Pumps, and Valves" section of Figure 1.5.
4. In the model, replace each tank with a reservoir. This is shown as step 4 in the "Implementing SCADA Data at Tanks, Pumps, and Valves" section of Figure 1.5.
5. Set the total head of each reservoir in the model to the value of head that was used to normalize the head at each hour and apply an hourly head pattern using the normalized heads calculated in step 3. Repeat this for all tanks. Now the head at the location of each

tank in the model should be equal to the head at each tank in the actual network for each hour. This is shown as step 5 in the "Implementing SCADA Data at Tanks, Pumps, and Valves" section of Figure 1.5.

Tank levels are directly related to system demands, as increased demands cause tanks to drain more rapidly. Often, system pump and valve operations are based on tank levels. Because of this, model demand uncertainty leads to uncertainty in model tank levels and model pump and valve operation. Forcing actual pump and valve operation and hourly tank levels in the model can reduce model error due to tank level and pump and valve operation uncertainty. For this study, the observed pump and valve operation and tank levels were taken from the outputs of the "real system" model and forced in the base model using time based operational controls and reservoirs with head patterns.

AMI data can be used directly as model inputs to match model demands to observed demands. When AMI data is available, the following steps should be taken to implement the data in a water distribution system model.

1. Collect hourly demand measurements from water meters throughout the network. This is shown as step 1 in the "Implementing AMI Data" section of Figure 1.5.
2. Identify nodes in the water distribution system model that carry demands. Then assign each meter to a demand node based on location. Meters can simply be assigned to the nearest demand node based on Euclidean distance, or can be assigned based on more advanced analyses involving unmodeled offshoot pipes. We assigned meters to demand nodes using Euclidean distance in this study. This is shown as step 2 in the "Implementing AMI Data" section of Figure 1.5.

3. For each demand node, sum the hourly demands of all of the meters assigned to that node for each hour. This will yield an observed total demand for each hour for each demand node. This is shown as step 3 in the "Implementing AMI Data" section of Figure 1.5.
4. Use the observed hourly total demands to normalize the demand at each node at each hour by dividing the total demand at each hour by a fixed value. This can be the average demand, maximum demand, or any other fixed value of demand. This is shown as step 4 in the "Implementing AMI Data" section of Figure 1.5.
5. Set the base demand of each demand node in the model to the value of demand that was used to normalize the demands at each hour and apply an hourly demand pattern using the normalized demands calculated in step 4. Repeat this for all demand nodes. Now the demand at each model demand node should be equal to the measured demand near each demand node location in the actual network for each hour. This is shown as step 5 in the "Implementing AMI Data" section of Figure 1.5.

Models built with two different sets of demands were used for this study. First, a base model was used to represent a hydraulic model that water managers would use without access to AMI data. The demands in this model represent average demands and were chosen based on water meter billing data. Typical diurnal demand patterns based on parcel-level land use information (residential, industrial, etc.) were applied to each demand node. These demands repeat after every 24 hour period, and were used as a baseline that we hoped to improve on.

Second, a model built with AMI data was considered to be representative of the real system. The demands in this model were measured hourly by Cary's AMI system during the month of March 2015. The physical components of the distribution system (i.e. nodes, pipes, tanks, pumps, and valves) and all model inputs except for demands are identical to the base

model. Because of this, all deviations from the "real system" model outputs seen in the base model outputs are due to demand uncertainty. Figure 1.7 shows the differences between the base model and "real system" model demands at a node over a week of simulation. Since this model was considered to be representative of the real system for the purposes of this study, the outputs from this model were treated like actual field measurements. Base model error was measured relative to the outputs from this "real system" model, with deviations from the pressures output from the "real system" model considered to be pressure error.

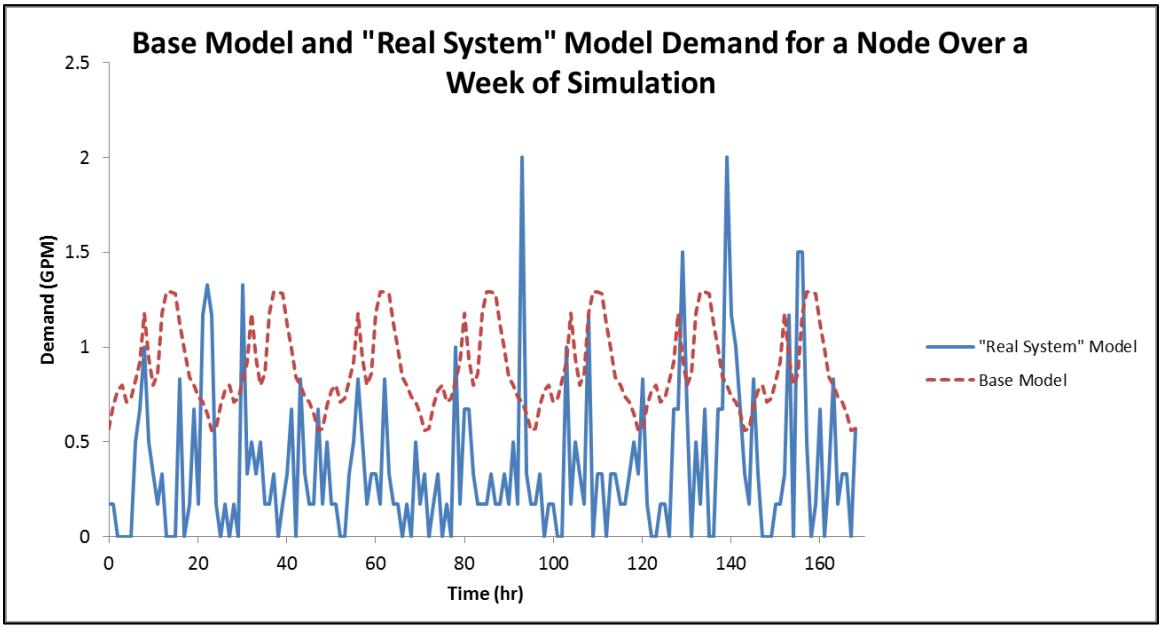

Figure 1.7. Differences in demand between the base model and "real system" model for a node over a week of simulation. The base model demands represent average demands with typical diurnal demand patterns based on water use that repeat every 24 hours. The "real system" model demands are actual demands measured by Cary's AMI system and aggregated to demand nodes.

Of the four types of data described, AMI data was used to develop the "real system" model and the other three types of data were employed in the base model both individually and in combination to quantify the resulting model improvement relative to the base model. The models developed by incorporating each data type are shown in Table 1.1. Root mean square error (RMSE) in pressure at model nodes between the "real system" model and the models built

by incorporating each data type with the base model was used to evaluate model performance in this study.

Table 1.1. Description of models developed by implementing PRV monitoring data, operational monitoring data, and SCADA data both individually and in combination. In the model names, "FN" stands for full network, "IN" stands for isolated network, "-D" indicates the application of a demand multiplier, and "-CR" indicates that controls have been matched and tanks have been replaced with reservoirs with head patterns.

Data Implemented	Model Name
AMI data	"Real System" Model
None – Base Model	FN
PRV monitoring	IN
Operational monitoring	FN-D
SCADA data	FN-CR
PRV monitoring + operational monitoring	IN-D
PRV monitoring + SCADA data	IN-CR
Operational monitoring + SCADA data	FN-DCR
PRV monitoring + operational monitoring + SCADA data	IN-DCR

1.4 Results and Discussion

To quantify model performance, first the pressure RMSE was calculated for the base model when compared to the "real system" model. Then PRV monitoring data, operational monitoring data, and SCADA data were all implemented in the base model both individually and in combination. The models resulting from implementing each data type are shown in Table 1.1 above. The resulting pressure RMSE from comparing each of the models to the "real system" model was then calculated, as shown in Equation 1.

$$RMSE = \sqrt{\frac{\sum_{i=1}^{n}\sum_{j=1}^{t}\left(P_{obs,i,j} - P_{\mathrm{mod}el,i,j}\right)^2}{n \times t}} \qquad (1)$$

Where P_{obs} is pressure output by the "real system" model and P_{model} is pressure output by the model of interest at node i and time step j. n represents the total number of nodes being compared and t represents the total number of time steps being compared.

For this study, only nodes in the western pressure zone were considered when calculating RMSE for each model. This was done so that the same nodes were compared for all models, as any

model incorporating PRV monitoring data consisted of only the nodes in the western pressure zone. The models were run for 24 hours of simulation, with model pressures output at each hour. The model improvement achieved by implementing each data type was calculated (base model pressure RMSE minus updated model pressure RMSE) and is presented in Figure 1.8.

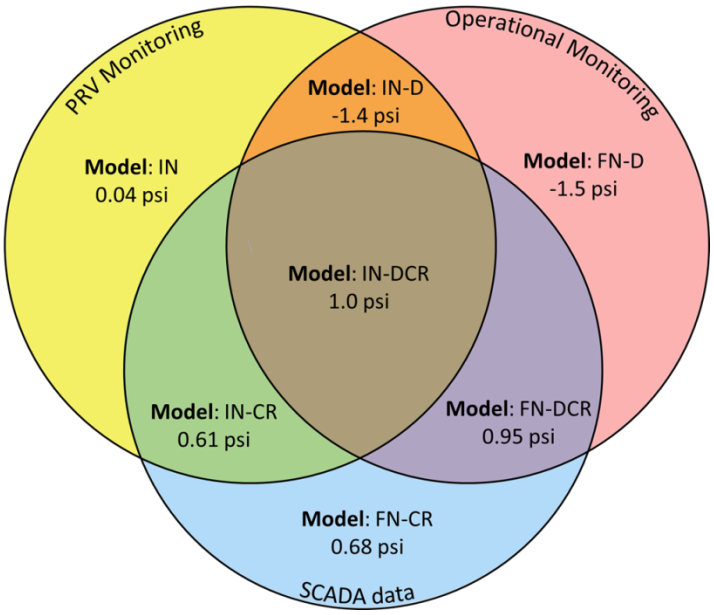

Figure 1.8. Models built using various data implementation strategies and their resulting RMSE improvement from the base model that implements none of this data. A negative RMSE improvement indicates that the model performed worse than the base model.

Implementing PRV monitoring data alone results in little model improvement over the base model. This is because adding a head boundary condition at the PRV only affects the model in hours that the PRV is open. In this case, the PRV that is modeled with a head boundary condition is only open for 5 hours out of the 24 total hours of simulation. When PRV monitoring data is implemented in combination with SCADA data, the resulting model performs better than the model that only incorporates PRV monitoring data. Though the model that incorporates both SCADA and PRV monitoring data performs worse overall than the model that incorporates SCADA data alone, the model that incorporates SCADA and PRV monitoring performs better at an increasing fraction of nodes as the PRV stays open longer. This trend holds true when

operational monitoring data is incorporated too. This temporal trend is illustrated in Figure 1.9. This indicates that we would see more model improvement from incorporating PRV monitoring data if the PRV was open for longer than 5 hours out of the day.

Incorporating PRV monitoring data most affects nodes hydraulically near the boundary condition. For our study, the PRV is open from 6 AM to 11 AM. At 7 AM, the pressures from the model incorporating PRV monitoring data along with SCADA and operational monitoring data are within 0.5 psi of the pressures from the model that only incorporates SCADA and operational monitoring data at most nodes, especially nodes far from the boundary condition. At the nodes near the boundary condition, the model that doesn't incorporate PRV monitoring data performs best. However, by 10 AM, after the PRV has been open for 4 hours, the model that incorporates PRV monitoring data performs best at nodes near the boundary condition. At the rest of the nodes, the pressures from the model that does and the model that doesn't incorporate PRV monitoring data are within 0.5 psi of each other. As time passes with the PRV open, the model improvement appears to spread outward from the PRV. These spatial and temporal trends are illustrated in Figure 1.10. Municipalities should take these spatial and temporal trends into consideration in their decision to invest in PRV monitoring data for model improvement purposes.

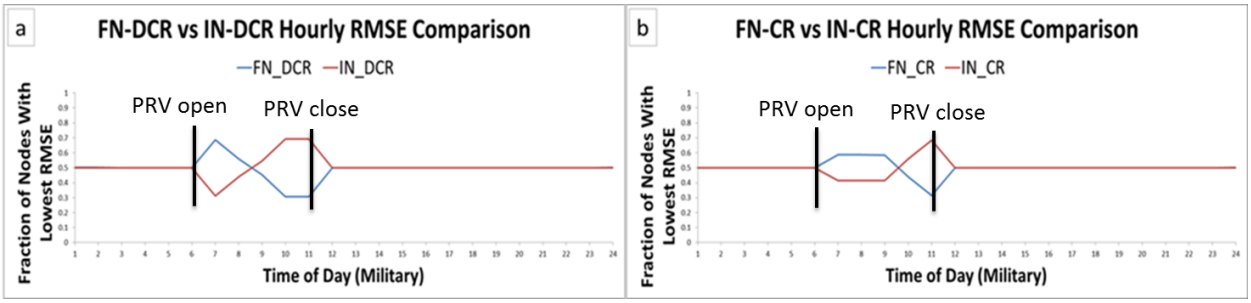

Figure 1.9. Temporal model comparison showing improvement resulting from PRV monitoring data (a) with operational monitoring data and (b) without operational monitoring data.

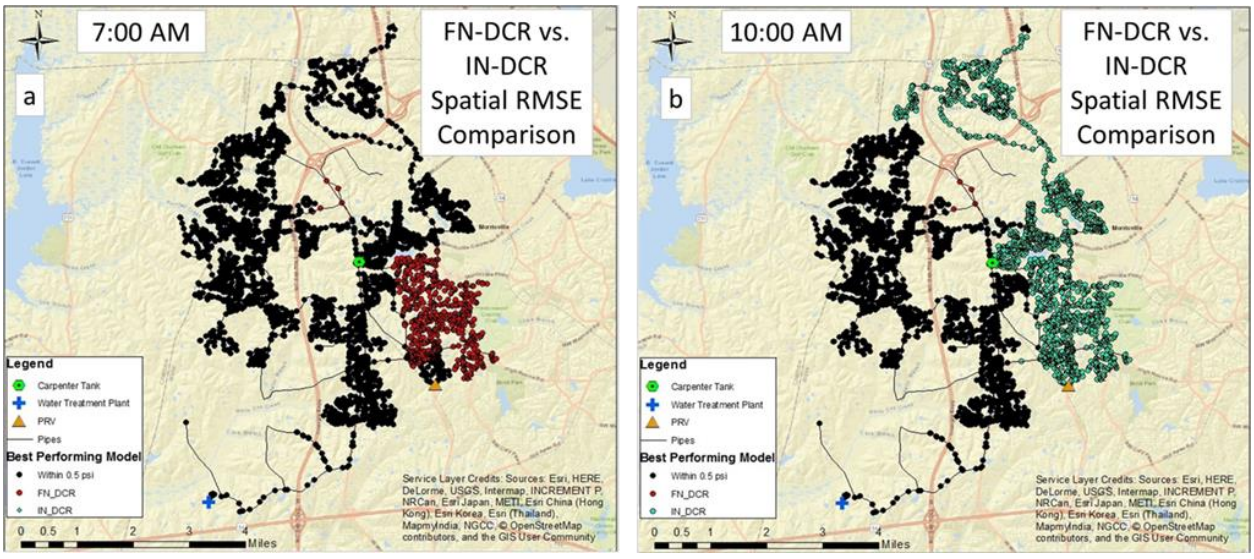

Figure 1.10. Spatial comparison highlighting model improvement in the western pressure zone from incorporating PRV monitoring data. In the model, the PRV is open from 6 AM to 11 AM. Comparisons are shown at (a) 7 AM and (b) 10 AM.

Implementing operational monitoring data alone and in combination with PRV monitoring data results in models that perform worse than the base model. Operational monitoring data only results in model improvement when it is paired with SCADA data. This indicates that municipalities shouldn't invest in collecting operational monitoring data for model improvement purposes without also investing in collecting SCADA data. When tank levels and pump and valve operations are matched, the temporal trend in model improvement resulting from incorporating operational monitoring data both with and without PRV monitoring data is shown in Figure 1.11.

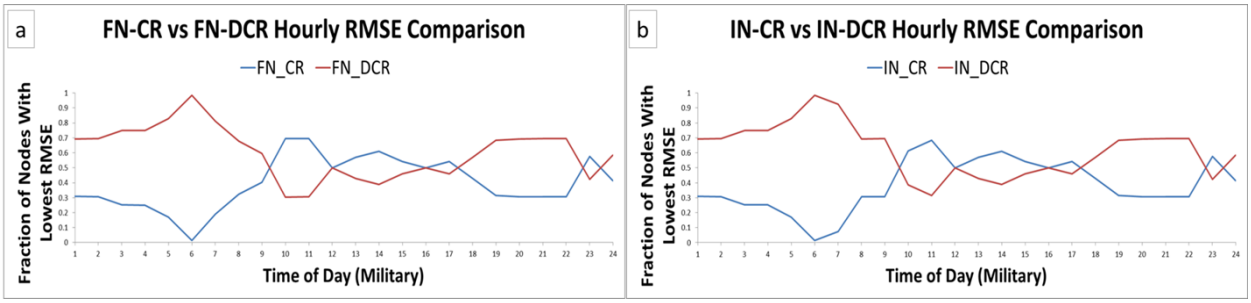

Figure 1.11. Temporal model comparison showing improvement resulting from implementing operational monitoring data in conjunction with SCADA data for (a) the full network model and (b) the isolated network model.

Of the three data types, implementing SCADA data results in the most model improvement. Pairing SCADA data with operational monitoring data results in a model that performs better than the models resulting from implementing SCADA or operational monitoring data alone. However, pairing SCADA data with PRV monitoring data results in a model that performs worse than the model that implements SCADA data alone. Of all the models tested, the model that incorporates all three data types showed the most improvement over the base model.

1.5 Conclusions

In this work, we have developed procedures to incorporate PRV monitoring data, operational monitoring data, SCADA system data, and AMI data into hydraulic models. We have also quantified the reduction in model error due to demand uncertainty resulting from the incorporation of three of these types of data into models and explored the spatial and temporal trends of the reduction in model error. The following conclusions can be drawn from this work.

- Reduction of model error can be achieved by the incorporation of data from PRV monitoring, operational monitoring, and SCADA systems into network models.
- Incorporating PRV monitoring data only affects the model during hours that the PRV is open. Model improvement from PRV monitoring data increases as the PRV reaches steady state. Model improvement is seen in areas hydraulically near the PRV.
- Incorporating operational monitoring data only results in model improvement when paired with SCADA data.
- Incorporating SCADA data results in the most model improvement of the three data types.
- The most model improvement is achieved by incorporating all three data types together.

Future work includes testing these data implementation procedures with more water distribution networks to verify that the findings presented here hold true. Also, types of model error other than demand error, such as pipe roughness error, should be considered.

CHAPTER 2

Modeling Chloramine Decay in Full Scale Drinking Water Supply Systems

Abstract

Chloramines are commonly used as secondary disinfectants in drinking water treatment, providing a residual for long lasting disinfection as drinking water moves through pipes to consumers. It is important for a desirable disinfection residual to be maintained throughout a distribution system to ensure that potentially harmful organisms present in the system are inactivated. Though chloramines are generally considered less reactive than free chlorine, they are inherently unstable, and undergo autodecomposition reactions even in the absence of reactive substances. In the presence of natural organic matter (NOM), chloramine loss is accelerated due to additional reaction pathways resulting in NOM oxidation. In this study, we have modeled chloramine loss due to autodecomposition and the presence of NOM in a batch system using MATLAB. The capabilities of the EPANET-MSX toolkit to model chloramine loss in a full scale water distribution network are also explored. A case study was carried out for the Town of Cary's water treatment facility and distribution network. First, a hydraulic model of Cary's water distribution system, which has about 27,000 nodes, was developed and calibrated using the EPANET toolkit with operational and water demand data supplied by Cary. Then water age from the calibrated hydraulic model was used in conjunction with the batch model of chloramine decay to successfully predict chloramine concentrations spatially and temporally throughout the network. The predicted concentrations can be used to identify locations that may need booster chloramines or chlorination in order to maintain a suitable disinfectant residual.

2.1 Introduction

The quality of drinking water is often reported based on samples taken at the clearwell of the water treatment plant. However, this quality inevitably undergoes changes while the water meanders through the distribution system to its final destination at consumers' taps. A distribution network acts as a chemical and biological reactor supported by biofilm growth in the aging infrastructure. The reactions that happen within it largely remain a black box. Water quality can be compromised in the distribution system with complications introduced by pressure drops, cross connections, contamination, breakage, and leakage (Kirmeyer et al., 2004). Therefore, it is very important to monitor and optimize the performance of the treatment not only within the treatment train, but also in the distribution network until the water reaches the farthest consumers' taps in order to ensure that the water supplied is in compliance with the required guidelines and standards.

The two secondary disinfectants that are most commonly used in drinking water treatment are chlorine and chloramine, mainly due to their ability to maintain residual concentrations long after the point of application. They not only inactivate the harmful pathogens that may be present in the finished water, but also suppress the microbial regrowth within water distribution networks, which may be naturally present or introduced by contamination. However, these secondary disinfectants introduced at the entry point to the distribution system can react with residual natural organic matter (NOM), pipe walls, and inorganics such as bromide, iodide, iron and nitrite that may still persist in the finished water. These reactions can produce unwanted halogenated disinfection by products (DBP), some of which are likely human carcinogens. Because of the proven ill-effects of DBPs, the US Stage 2 Disinfectants and Disinfection Byproducts Rule (D/DBP Rule) requires water utilities to comply with a maximum

contaminant level (MCL) of 80 µg/L for trihalomethanes (THM) and an MCL of 60 µg/L for five haloacetic acids (HAA5) as the running annual average at individual locations in a distribution system (USEPA, 2010). These stringent drinking water regulations have prompted utilities to switch to chloramine as a secondary disinfectant since chloramines are more stable, less reactive and more persistent than free chlorine and therefore have the tendency to form significantly lower levels of THM and HAA5.

Chloramines are produced by a reaction between chlorine and free ammonia that can result in monochloramine (NH_2Cl), dichloramine ($NHCl_2$) and trichloramine (NCl_3). The relative amounts of each of these species are dependent on pH, temperature, contact time, and the ratio between Cl_2:NH_3-N. In typical water distribution systems, monochloramine is the dominant and preferred species produced for secondary disinfection because of its biocidal properties, relative stability, and relatively lower taste and odor properties. Chloramine that is formed at the entry point of a distribution system slowly undergoes decay within the distribution system due to autodecomposition and ongoing reactions with natural organic matter and inorganics. While chloramine is less reactive than free chlorine in producing regulated DBPs in combination with organics, it still forms some DBPs. Recently, there have been concerns regarding emerging disinfection by-products such as N-Nitrosodimethaylamine (NDMA) being formed by chloramine.

When chloramine undergoes decay due to autodecomposition and reactions with NOM, the main product of the reactions is ammonia, which has the potential to promote nitrification reactions by autotrophic bacteria whenever the residual chloramine concentration falls below 2 mg/L within distribution systems having higher residence times (Wilczak et al., 1996). Nitrification can have the adverse impacts of increasing nitrite and nitrate levels, reducing

alkalinity, pH, dissolved oxygen and chloramine residuals and promoting bacterial regrowth (Wilczak et al., 1996). The occurrence of nitrification accompanied by a decrease in pH can promote the corrosion of infrastructure (Zhang et al., 2008). Once the nitrification is initiated at a segment of pipe, then chloramine decay can be further accelerated causing the loss of disinfectant (Sawade et al., 2015). Since the concentration of chloramine residual can vary temporally and spatially due to a myriad of reactions, the management of chloramine residuals within a distribution system is a major concern.

Intensive monitoring of the water quality for the desired constituents in vulnerable locations within the distribution network can serve to address this concern partially. The water quality parameters that are required to be measured within distribution systems at a certain frequency and at specified locations include chlorine/chloramine residual, coliform, and DBP concentrations (regulated contaminants). When routine measurements trigger a concern, for example, when chloramine concentration is not detectable, other measurements such as total ammonia and nitrite concentrations, along with other parameters, may be monitored (Kirmeyer et al., 2004). Real-time monitoring of certain contaminants is currently implemented within treatment plants for process control purposes. However, it has been a challenge to incorporate real-time measurement of water quality after the water leaves the distribution system and take any corrective actions needed due to high capital cost for the installation of state-of-the art instrumentation in critical locations (Kirmeyer et al., 2004).

The U.S. Environmental Protection Agency (EPA) requires most community water systems to provide customers with an annual water quality report. The report gives the average water quality at the water treatment plant and DBPs in certain locations within the distribution system as a running annual average (USEPA, 2010). However, this annually aggregated quality

report gives limited information regarding temporal and spatial variation of water quality in real time. Temporal and spatial water quality information within a distribution system can only be realized by well-calibrated modelling, which can then be used to predict concentrations. Precise quality modeling in a distribution system requires a robust and accurate hydraulic model and the availability of calibrated quality models of interest.

Several researchers have been working on developing kinetic models for the autodecomposition of chloramine in which chloramine undergoes a complex set of reactions and produces ammonia and nitrogen as final products. Vikesland et al (2001) worked on the validation of the previously developed models (Jafvert and Valentine, 1992; Ozekin et al., 1996) under realistic water quality and chloramination conditions and the incorporation of temperature dependencies of important reactions. The kinetic parameters in these models were further improved and validated with various environmental conditions such as pH, temperature and initial chlorine to ammonia molar ratio (Cl_2/N) using the data obtained from the lab scale experiments conducted in the previous literature (Huang, X, 2008). Further, chloramine loss in the presence of organic matter was investigated by Duirk et al (2005) in which the reaction was described as bi-phasic using four NOM specific reaction parameters. DBP formation during chloramination was also investigated and a comprehensive model was further developed incorporating the effect of bromide and chlorine containing dihaloacetic acids in the presence of natural organic matter by Duirk and Valentine (2007). Zhu and Zhang et al (2016) recognized the fact that the use of chlorine and chloramine in drinking water disinfection can produce numerous halogeneated DBPs depending on the presence of precursors in the raw/treated water, and they emphasized total organic halogen (TOX) as a collective parameter and its disaggregation such as total organic chlorine (TOCl), total organic bromine (TOBr) and total

organic iodine (TOI) need to be evaluated as opposed to THMs and HAA5. They modeled the formation kinetics of TOCl, TOBr and TOI. Zhu and Zhang et al (2016) developed the formation kinetics of TOCl, TOBr and TOI both on chlorination and chloramination by selecting a series of bromine and iodine related reactions. These models accurately predicted the levels of TOX along with total chlorine residual for simulated raw waters and are very valuable since these are based on kinetic reactions as opposed to statistical or empirical or power based models based on water qualities. However, the kinetic parameters proposed in Zhu and Zhang (2016) need further validation for wide ranging environmental conditions in real water before application. Overall, while these models on chloramine decay have been developed in lab-scale batch systems, their usefulness cannot be realized unless they are applied for a large scale distribution system.

EPANET is a widely used program for modeling the hydraulic and water quality behavior of drinking water distribution systems. The recently developed software tool EPANET-MSX (multi-species extension) by Shang et al (2008) claims to accurately model multi-species water quality issues within a distribution system. EPANET-MSX enables the computation of the individual chemical species in discrete parcels of water as these parcels are transported through the network pipes by the bulk velocity using Lagrangian model (Shang et al., 2008) using flows generated by a well calibrated hydraulic model (e.g., EPANET hydraulic model). There have been some attempts to model the chlorine decay via two–reactant second order decay model using EPANET-MSX (Monteiro et al, 2014; Ohar and Ostfeld, 2014), but there have been none attempting to model the chloramine decay in a large scale distribution system for the purpose of predicting the residual disinfectants spatially and temporally. Therefore, the objectives of this investigation are 1) model chloramine loss due to

autodecomposition and the presence of natural organic matter in a batch system and validate the model 2) develop and calibrate a hydraulic model for a large-scale distribution system using EPANET 3) use water age from the calibrated hydraulic model together with the batch system model to predict chloramine concentrations spatially and temporally 4) explore the capabilities of the EPANET-MSX toolkit to model chloramine loss in a full scale water distribution network.

2.2 Batch Reaction Model Development

We adopted models for chloramine decay due to autodecomposition alone (autodecomposition model) and chloramine decay due to autodecomposition and the presence of NOM (autodecomposition + DOC model) for eventual application in a full scale drinking water supply system. The autodecomposition model and the autodecomposition + DOC model are described in detail in section 2.1 and 2.2 respectively.

2.2.1 Model Depicting Autodecomposition of Chloramine

The chloramine decay due to autodecomposition model contains 19 reactions, as described in Table 2.1. The kinetic coefficients of these reactions were calibrated and validated with various environmental conditions with pH ranging from 6.5 to 9.5, temperature ranging from 4 to 30 ^{o}C, total carbonate buffer concentration ranging from $9x10^{-4}$ to $1x10^{-2}$ M, and initial chlorine to ammonia molar ratios (Cl_2/N) ranging from 0.5 to 2.0 (Vikesland et al. 2001, Huang, X, 2008), describing realistic quality and chloramination conditions. Therefore, these rates were adopted for the autodecomposition model.

Table 2.1. Chloramine autodecomposition model.

No.	Reaction Stoichiometry	Rate Coefficient/Equilibrium Constant	Reference
1	$HOCl + NH_3 \longrightarrow NH_2Cl + H_2O$	$k_1 = 2.37\times10^{12}\exp\left(-\frac{1510}{T}\right)M^{-1}h^{-1}$	Morris and Issac, 1981 cited in Vikesland et al, 2001
2	$NH_2Cl + H_2O \longrightarrow HOCl + NH_3$	$k_2 = 6.7\times10^{11}\exp\left(-\frac{8800}{T}\right)h^{-1}$	Morris and Issac, 1981 cited in Vikesland et al, 2001
3	$HOCl + NH_2Cl \longrightarrow NHCl_2 + H_2O$	$k_3 = 1.08\times10^{9}\exp\left(-\frac{2010}{T}\right)M^{-1}h^{-1}$	Margerum et al, 1978 cited in Vikesland et al, 2001
4	$NHCl_2 + H_2O \longrightarrow HOCl + NH_2Cl$	$k_4 = 2.3\times10^{-3}h^{-1}$	Margerum et al, 1978 cited in Vikesland et al, 2001
5	$NH_2Cl + NH_2Cl \longrightarrow NHCl_2 + NH_3$	$k_5 = k_{5,H}\left[H^+\right] + k_{5,HCO3}\left[HCO_3^-\right] + k_{5,H2CO3}\left[H_2CO_3\right]$	Vikesland et al, 2001
		$k_{5,H} = 3.78\times10^{10}\exp\left(-\frac{2169}{T}\right)M^{-2}h^{-1}$	Granstrom, 1954 cited in Vikesland et al, 2001
		$k_{5,HCO3} = 1.5\times10^{35}\exp\left(-\frac{22144}{T}\right)M^{-2}h^{-1}$	Vikesland et al, 2001
		$k_{5,H2CO3} = 2.95\times10^{10}\exp\left(-\frac{4026}{T}\right)M^{-2}h^{-1}$	Vikesland et al, 2001
6	$NHCl_2 + NH_3 \longrightarrow NH_2Cl + NH_2Cl$	$k_6 = 2.2\times10^{8}M^{-2}h^{-1}$	Hand and Margerum, 1983 cited in Vikesland et al, 2001
7	$NHCl_2 + H_2O \longrightarrow NOH^a + 2HCl^b$	$k_7 = 4.0\times10^{5}M^{-1}h^{-1}$	Reaction from Huang, 2008 Rate coefficient from Jafvert and Valentine, 1987 cited in Vikesland et al, 2001
8	$NOH^a + NHCl_2 \longrightarrow HOCl + N_2^b + HCl^b$	$k_8 = 1.0\times10^{8}M^{-1}h^{-1}$	Jafvert, 1985 cited in Huang, 2008
9	$NOH^a + NH_2Cl \longrightarrow N_2^b + HCl^b + H_2O^b$	$k_9 = 3.0\times10^{7}M^{-1}h^{-1}$	Jafvert, 1985 cited in Huang, 2008
10	$NH_2Cl + NHCl_2 \longrightarrow N_2^b + 3HCl^b$	$k_{10} = 55.0M^{-1}h^{-1}$	Reaction from Huang, 2008 Rate coefficient from Leao, 1981 cited in Vikesland et al, 2001

Table 2.1 (continued).

11	$HOCl + NHCl_2 \longrightarrow NCl_3 + H_2O$	$k_{11} = k_{11,OH}\left[OH^-\right] + k_{11,OCl}\left[OCl^-\right] + k_{11,CO3}\left[CO_3\right]$	Hand and Margerum, 1983 cited in Huang, 2008
		$k_{11,OH} = 1.18\times10^{13}\,M^{-2}h^{-1}$	Hand and Margerum, 1983 cited in Huang, 2008
		$k_{11,OCl} = 3.24\times10^{8}\,M^{-2}h^{-1}$	Hand and Margerum, 1983 cited in Huang, 2008
		$k_{11,CO3} = 2.16\times10^{10}\,M^{-2}h^{-1}$	Hand and Margerum, 1983 cited in Huang, 2008
12	$NHCl_2 + NCl_3 + 2H_2O \longrightarrow 2HOCl + N_2^b + 3HCl^b$	$k_{12} = 3.6\times10^{17}\,M^{-2}h^{-1}$	Huang, 2008
13	$NH_2Cl + NCl_3 + H_2O \longrightarrow HOCl + N_2^b + 3HCl^b$	$k_{13} = 3.6\times10^{9}\,M^{-2}h^{-1}$	Huang, 2008
14	$NHCl_2 + 2HOCl + H_2O \longrightarrow NO_3^- + 5H^+ + 4Cl^-$	$k_{14} = 2.38\times10^{5}\,M^{-2}h^{-1}$	Huang, 2008
15	$NCl_3 + H_2O \longrightarrow NHCl_2 + HOCl$	$k_{15} = k_{15,0} + k_{15,1}\left[OH^-\right] + k_{15,2}\left[OH^-\right]^2 + k_{15,HCO3}\left[HCO_3^-\right]\left[OH^-\right]$	Kumar et al, 1987 cited in Huang, 2008
		$k_{15,0} = 5.76\times10^{-3}\,h^{-1}$	Kumar et al, 1987 cited in Huang, 2008
		$k_{15,1} = 2.88\times10^{4}\,h^{-1}$	Kumar et al, 1987 cited in Huang, 2008
		$k_{15,2} = 3.20\times10^{6}\,h^{-1}$	Kumar et al, 1987 cited in Huang, 2008
		$k_{15,HCO3} = 2.34\times10^{5}\,M^{-2}h^{-1}$	Kumar et al, 1987 cited in Huang, 2008
16	$HOCl \longleftrightarrow H^+ + OCl^-$	$pK_{a1} = 1.18\times10^{-4}\left(T\right)^2 - 7.86\times10^{-2}\left(T\right) + 20.5$	Morris, 1966 cited in Vikesland et al, 2001
17	$NH_4^+ \longleftrightarrow NH_3 + H^+$	$pK_{a2} = 1.03\times10^{-4}\left(T\right)^2 - 9.21\times10^{-2}\left(T\right) + 27.6$	Bates and Pinching, 1949 cited in Vikesland et al, 2001
18	$H_2CO_3 \longleftrightarrow HCO_3^- + H^+$	$pK_{a3} = 1.48\times10^{-4}\left(T\right)^2 - 9.39\times10^{-2}\left(T\right) + 21.2$	Snoeyink and Jenkins, 1980 cited in Vikesland et al, 2001

Table 2.1 (continued).

19	$HCO_3^- \longleftrightarrow CO_3^{2-} + H^+$	$pK_{a4} = 1.19\times10^{-4}\left(T\right)^2 - 7.99\times10^{-2}\left(T\right) + 23.6$	Snoeyink and Jenkins, 1980 cited in Vikesland et al, 2001

All T in Kelvin

[a] Assumed formula for the unidentified intermediate

[b] Products and stoichiometry are assumed for balancing the reaction. Possible products may include N_2, H_2O, Cl^-, H^+, NO_3^- and other unidentified reaction products

2.2.2 Model Depicting Autodecomposition in the Presence of DOC

The model developed by Duirk et al. (2005) was incorporated to include chloramine loss due to the presence of NOM, as described in Figure 2.1. Additions made to the autodecomposition model to account for the oxidation of NOM are shown in Table 2.2. The reaction of chloramine with NOM was described as biphasic using four NOM specific reaction parameters. NOM pathway 1 involves the direct reaction of monochloramine with NOM (k_{DOC1}) and pathway 2 is slower and attributable to free chlorine (k_{DOC2}) derived from monochloramine loss. S_1 and S_2 are parameters that represent the fast and slow percentage of reactive sites in the NOM structure that exhibit reactivity with monochloramine or free chlorine respectively.

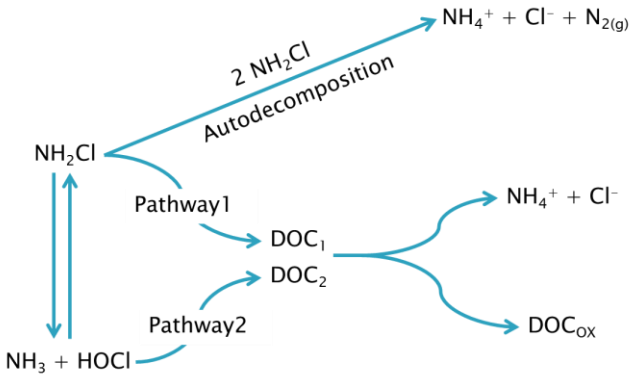

Figure 2.1. Depiction of monochloramine reaction pathways in the presence of NOM, adopted from Duirk et al (2005). DOC_{OX} represents oxidized NOM.

Table 2.2. Additions to the chloramine decomposition model to account for the oxidation of NOM.

No.	Reaction Stoichiometry	Rate Coefficient/Equilibrium Constant	Reference
20	$NH_2Cl + DOC_1 \longrightarrow$ Products	k_{DOC1}	Duirk et al, 2005
21	$HOCl + DOC_2 \longrightarrow$ Products	k_{DOC2}	Duirk et al, 2005

Where $DOC_1 = \frac{TOC \times S_1}{12,000}$ and $DOC_2 = \frac{TOC \times S_2}{12,000}$

2.2.3 Solution Approach

This water quality model was converted to a system of differential algebraic equations (DAE) consisting of differential equations for kinetic reactions (equations 1-11 presented in Table 2.5

later) and algebraic equations for equilibrium reactions (equations 12-15 presented in Table 2.5 later). The reaction rates for the autodecomposition model are shown in Table 2.3 and the reaction rates added to account for the oxidation of NOM are shown in Table 2.4. The k values referred to in the "Rate" section of Table 2.3 can be found in Table 2.1. The reaction kinetics for each species in the autodecomposition model are shown in Table 2.5 and the updated reaction kinetics to account for the oxidation of NOM are shown in Table 2.6.

Table 2.3. Reactions and rates for autodecomposition system. K values referred to under "Rate" can be found in Table 2.1.

Reaction	Rate
$HOCl + NH_3 \longrightarrow NH_2Cl + H_2O$	$a_1 = k_1[HOCl][NH_3]$
$NH_2Cl + H_2O \longrightarrow HOCl + NH_3$	$a_2 = k_2[NH_2Cl]$
$HOCl + NH_2Cl \longrightarrow NHCl_2 + H_2O$	$a_3 = k_3[HOCl][NH_2Cl]$
$NHCl_2 + H_2O \longrightarrow HOCl + NH_2Cl$	$a_4 = k_4[NHCl_2]$
$NH_2Cl + NH_2Cl \longrightarrow NHCl_2 + NH_3$	$a_5 = k_5[NH_2Cl][NH_2Cl]$
$NHCl_2 + NH_3 \longrightarrow NH_2Cl + NH_2Cl$	$a_6 = k_6[NHCl_2][NH_3][H^+]$
$NHCl_2 + H_2O \longrightarrow NOH^a + 2HCl^b$	$a_7 = k_7[NHCl_2][OH^-]$
$NOH^a + NHCl_2 \longrightarrow HOCl + N_2^b + HCl^b$	$a_8 = k_8[NOH][NHCl_2]$
$NOH^a + NH_2Cl \longrightarrow N_2^b + HCl^b + H_2O^b$	$a_9 = k_9[NOH][NH_2Cl]$
$NH_2Cl + NHCl_2 \longrightarrow N_2^b + 3HCl^b$	$a_{10} = k_{10}[NH_2Cl][NHCl_2]$
$HOCl + NHCl_2 \longrightarrow NCl_3 + H_2O$	$a_{11} = k_{11}[HOCl][NHCl_2]$
$NHCl_2 + NCl_3 + 2H_2O \longrightarrow 2HOCl + N_2^b + 3HCl^b$	$a_{12} = k_{12}[NHCl_2][NCl_3][OH^-]$
$NH_2Cl + NCl_3 + H_2O \longrightarrow HOCl + N_2^b + 3HCl^b$	$a_{13} = k_{13}[NH_2Cl][NCl_3][OH^-]$
$NHCl_2 + 2HOCl + H_2O \longrightarrow NO_3^- + 5H^+ + 4Cl^-$	$a_{14} = k_{14}[NHCl_2][OCl^-]$
$NCl_3 + H_2O \longrightarrow NHCl_2 + HOCl$	$a_{15} = k_{15}[NCl_3]$

Table 2.4. Additional reactions to account for the oxidation of NOM.

Reaction	Rate
$NH_2Cl + DOC_1 \longrightarrow$ Products	$a_{16} = k_{DOC1}[DOC_1][NH_2Cl]$
$HOCl + DOC_2 \longrightarrow$ Products	$a_{17} = k_{DOC2}[DOC_2][HOCl]$

Where $DOC_1 = \frac{TOC \times S_1}{12,000}$ and $DOC_2 = \frac{TOC \times S_2}{12,000}$

Table 2.5. Reaction kinetics for autodecomposition DAE system.

No.	Species	Reaction Equations
1	Free Cl_2	$\frac{d[HOCl]}{dt} = -a_1 + a_2 - a_3 + a_4 + a_8 - a_{11} + 2a_{12} + a_{13} - 2a_{14} + a_{15}$
2	Free N	$\frac{d[NH_3]}{dt} = -a_1 + a_2 + a_5 - a_6$
3	NH_2Cl	$\frac{d[NH_2Cl]}{dt} = a_1 - a_2 - a_3 + a_4 - 2a_5 + 2a_6 - a_9 - a_{10} - a_{13}$
4	$NHCl_2$	$\frac{d[NHCl_2]}{dt} = a_3 - a_4 + a_5 - a_6 - a_7 - a_8 - a_{10} - a_{11} - a_{12} - a_{14} + a_{15}$
5	Unknown intermedate (NOH)	$\frac{d[NOH]}{dt} = a_7 - a_8 - a_9$
6	NCl_3	$\frac{d[NCl_3]}{dt} = a_{11} - a_{12} - a_{13} - a_{15}$
7	Cl^-	$\frac{d[Cl^-]}{dt} = 2a_7 + a_8 + a_9 + 3a_{10} + 3a_{12} + 3a_{13} + 4a_{14}$
8	N_2	$\frac{d[N_2]}{dt} = a_8 + a_9 + a_{10} + a_{12} + a_{13}$
9	NO_3^-	$\frac{d[NO_3^-]}{dt} = a_{14}$
10	HCO_3^-	$\frac{d[HCO_3^-]}{dt} = [Alk] - [HCO_3^-] - 2[CO_3] - [OH^-] + [H^+]$
11	OH^-	$\frac{d[OH^-]}{dt} = [H^+][OH^-] - 10^{-14}$
12	OCl^-	$[OCl^-] = \frac{K_{a1}[HOCl]}{[H^+]}$
13	NH_4^+	$[NH_4^+] = \frac{[H^+][NH_3]}{K_{a2}}$
14	CO_3^{2-}	$[CO_3^{2-}] = \frac{K_{a4}[HCO_3^-]}{[H^+]}$
15	H_2CO_3	$[H_2CO_3] = \frac{[H^+][HCO_3^-]}{K_{a3}}$

Table 2.6. Updated reaction kinetics for autodecomposition + DOC DAE system.

No.	Species	Reaction Kinetics
19	Free Cl_2	$\frac{d[HOCl]}{dt} = -a_1 + a_2 - a_3 + a_4 + a_8 - a_{11} + 2a_{12} + a_{13} - 2a_{14} + a_{15} - a_{17}$
20	Free N	$\frac{d[NH_3]}{dt} = -a_1 + a_2 + a_5 - a_6 + a_{16}$
21	NH_2Cl	$\frac{d[NH_2Cl]}{dt} = a_1 - a_2 - a_3 + a_4 - 2a_5 + 2a_6 - a_9 - a_{10} - a_{13} - a_{16}$
22	DOC_1	$\frac{d[DOC_1]}{dt} = -a_{16}$
23	DOC_2	$\frac{d[DOC_2]}{dt} = -a_{17}$

Table 2.7 gives the initial conditions adopted in this study. These were extracted from data given by the Town of Cary for the month of August 2017. The average values of temperature, pH, total alkalinity, TOC, free chlorine, and ammonia were computed for August 2017 in the finished water for adoption in this work. The S_1 and S_2 values that are needed to find the DOC_1 and DOC_2 fractions present in the NOM should have been ideally obtained from kinetic experiments conducted with Cary's water. However, for the purpose of this work, S_1 and S_2 values were obtained through model calibration.

Table 2.7. Initial conditions adopted for this study.

Parameter	Initial Condition
Temperature	29º C
pH	7.71
Total Alkalinity Concentration	8.00E-4 eq/L as $CaCO_3$
Total Organic Carbon Concentration	2.00E-4 M as C
Free Cl_2 Concentration	5.57E-5 M
Ammonia Concentration	7.50E-5 M
S_1	0.016
S_2	0.57
DOC_1	3.20E-6
DOC_2	1.14E-4

2.3 Town of Cary Case Study

A case study was carried out to the Cary/Apex Water Treatment Facility and distribution system. This water treatment facility has a capacity of 40 million gallons per day (MGD) and serves water to the Town of Cary, the Town of Morrisville, the Wake County portion of Research Triangle Park (RTP), and the Raleigh-Durham (RDU) International Airport. The Town of Cary's water distribution system is shown in Figure 2.2, with the location of the Cary/Apex Water Treatment Facility indicated.

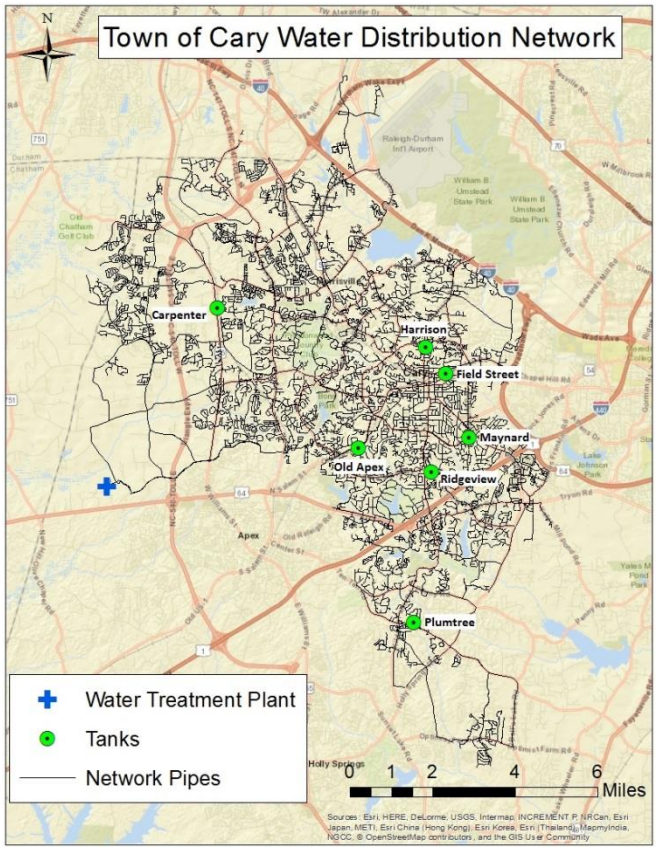

Figure 2.2. Map of Cary's water distribution system with the location of tanks indicated with green circles, pipes indicated with black lines, and the Cary/Apex Water Treatment Facility indicated with a blue cross. Tanks are labeled by name.

2.3.1 Description of Cary's Water Treatment System

The Cary/Apex Water Treatment Facility extracts raw water from Jordan Lake, which is part of the Cape Fear River basin. First, powdered activated carbon (PAC) is added to the raw water

and the water is pumped six miles from the lake to the treatment facility. Once the water reaches the treatment facility, ozone is used to oxidize organics and remove color, taste, and odors present in the raw water. Subsequently, water undergoes a coagulation process in the rapid mixing tank, where aluminum sulfate and polymer are added to enhance the floc formation and agglomeration, respectively. The flocculated water is then subjected to clarification using pulsators, and the settled water that exits the pulsators is subjected to optional additional ozonation. As the water flows from the pulsators to the filters, chlorine in the form of liquid bleach is added as a primary disinfectant. The water then undergoes sand and carbon filtration, where additional particles are removed from the water. After filtration, post-treatment measures such as pH adjustment and fluoride addition are taken and the treated water is sent to clearwells for storage. In the clearwells, the water is subjected to secondary disinfection before distribution. Chlorine and ammonia are added in order to form desired chloramine residuals at the entry point to the distribution system.

The average raw and finished water quality at the Cary/Apex Water Treatment Facility is presented in Table 2.8. Water quality for August 2017 is listed because the case study was carried out for that month.

Table 2.8. Quality of raw and finished water at the Cary/Apex Water Treatment Facility.

	Raw Water		**Finished Water**	
	Average	Aug 2017	Average	Aug 2017
pH	7.08	7.04	7.70	7.71
Turbidity (NTU)	16.64	10.01	0.60	0.64
Alkalinity (mg $CaCO_3$/L)	34.04	39.31	35.96	41.23
Hardness (mg $CaCO_3$/L)	32.06	33.60	32.02	32.97
Iron (max) (mg/L)	0.26	0.12	0.01	0.00
Manganese (mg/L)	0.19	0.29	0.01	0.01
TOC (mg C/L)	6.82	6.93	2.32	2.40
Bromide (mg/L)	0.099	N/A	N/A	N/A
Bromate (mg/L)	N/A	N/A	0.0015	N/A

2.3.2 Hydraulic Model Development and Calibration

The Town of Cary has invested in an advanced metering infrastructure (AMI) system to take hourly water meters readings remotely. Close to 60,000 AMI water meters have been installed in the water distribution system. Hourly data for the month of August 2017 from each AMI meter was provided by the Town of Cary to assist this project. The data provided for each meter includes meter location, service (i.e. potable, irrigation, reclaimed), size, jurisdiction, time of each reading, and water consumption for each hour with a resolution of ten gallons (i.e. every tenth gallon that is consumed is reported). In addition to the hourly water demand data, data from Cary's supervisory control and data acquisition (SCADA) system including hourly tank level, pump operation, and pressure and flow at several points throughout the system was provided for August 2017. This data was used in conjunction with a hydraulic planning model developed by the private contracting company CH2M HILL to build a hydraulic model of the Town of Cary's water distribution system for August 2017. CH2M HILL built the planning model for the Town of Cary in 2009 using the EPANET software toolkit. In this project, physical components of the distribution system (i.e. pipes, nodes, tanks, pumps, and valves) were taken from the previously developed planning model, and the demands and operational controls were determined based on the August 2017 data provided by Cary. This project represents the first attempt to use SCADA data in conjunction with AMI data to build an operational model of Cary's water distribution system.

Meter demands were aggregated to the nearest model demand nodes using the k-nearest neighbors algorithm (knnsearch function in MATLAB). Model demand nodes were considered to be the nodes that carry demands in the planning model developed by CH2M HILL. Operational controls were set for the model so that the level of each tank cycled over a

reasonable range for a month of simulation when compared to the tank level data collected by the SCADA system. Two examples of model tank levels compared to tank levels reported by the SCADA system are shown in Figure 2.3. Additional figures showing model tank levels compared to tank levels reported by the SCADA system are included as Appendix A. The level of the Harrison Tank was not recorded during August 2017 due to an error with the SCADA system.

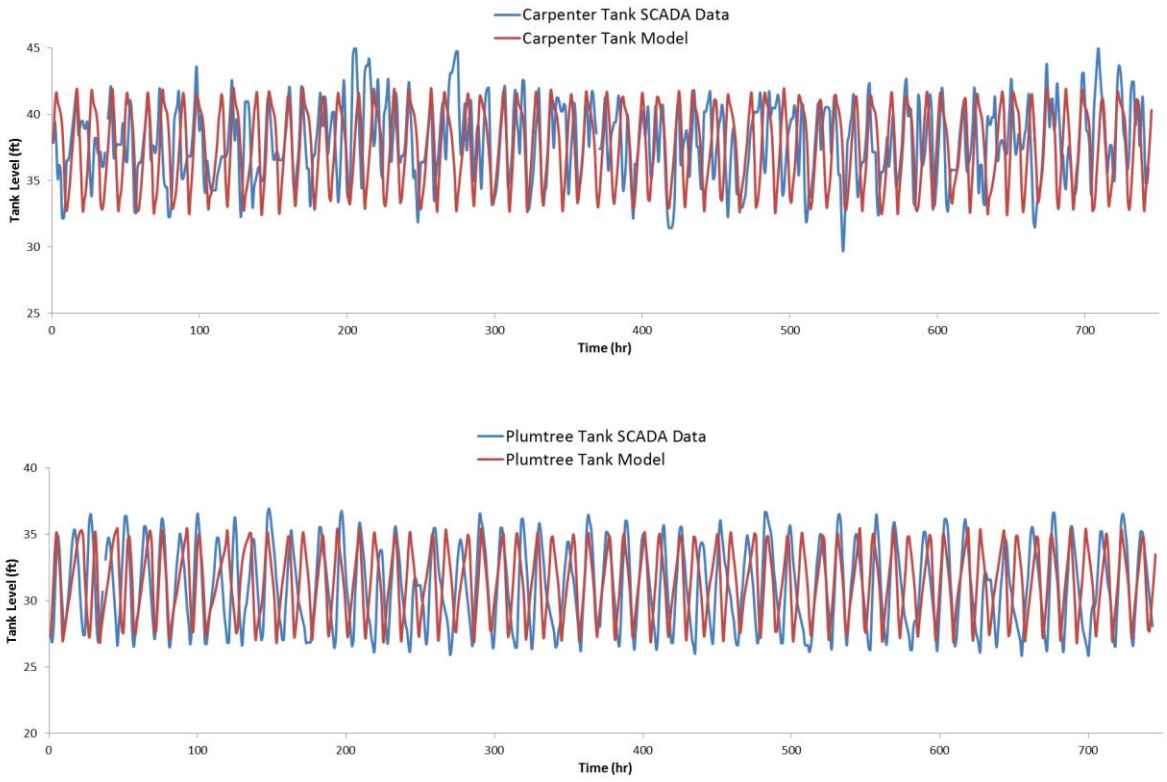

Figure 2.3. August 2017 tank levels measured with SCADA compared to tank levels from the calibrated hydraulic model for the Carpenter Tank (top) and Plumtree Tank (bottom).

2.4 Results and Discussion

2.4.1 Overview of Models Developed

Seven models were developed for this project, each representing a step towards modeling chloramine decay due to autodecomposition and the presence of NOM in a full scale water

distribution system. Models were applied for two chloramine decay scenarios, first decay due to autodecomposition alone and second decay due to autodecomposition and the presence of NOM. For each of the two decay scenarios, three hydraulic scenarios were modeled. First, models were built for a batch reaction system using MATLAB's differential algebraic equation (DAE) solver ode15s. Second, models were built for a simple water distribution network consisting of five pipes and four nodes using the EPANET-MSX toolkit. Finally, models were built for the Town of Cary's water distribution network, which contains 28331 pipes and 26986 nodes, using the EPANET-MSX toolkit. The decay scenario due to autodecomposition and NOM is more complex to model than the decay scenario due to autodecomposition alone. The batch reaction system is the simplest hydraulic modeling scenario, and the simple distribution network and Town of Cary distribution network represent increasing modeling complexity, respectively. The seventh model paired the batch reaction system model of chloramine decay due to autodecomposition and NOM with the water ages output from a calibrated EPANET hydraulic model of Cary's distribution network. The batch reaction system model predicts chloramine concentration as a function of water age, so the water age reported at nodes of interest can be used to find corresponding chloramine concentrations for those nodes. The seven models developed are shown in Table 2.9.

Table 2.9. Chloramine decay models developed for this project. Each model represents an additional step towards modeling chloramine decay due to autodecomposition and the presence of NOM in a full-scale water distribution network.

No.	Model Name	Description
1	Auto-Batch	Autodecomposition model with batch reaction system
2	AutoDOC-Batch	Autodecomposition + DOC model with batch reaction system
3	Auto-MSX-Simple	Autodecomposition model with EPANET-MSX for simple hydraulic network
4	Auto-MSX-Cary	Autodecomposition model with EPANET-MSX for Cary's hydraulic network
5	AutoDOC-MSX-Simple*	Autodecomposition + DOC model with EPANET-MSX for simple hydraulic network
6	AutoDOC-MSX-Cary*	Autodecomposition + DOC model with EPANET-MSX for Cary's hydraulic network
7	AutoDOC-Batch w/ water age from Cary EPANET	Autodecomposition + DOC model with batch reaction system paired with water age from calibrated hydraulic model of Cary's network

*Model produces unexpected results, not used

2.4.2 Batch Model Validation

The batch system models were solved using MATLAB's ode15s solver. Models were validated against a batch reactor simulation of chloramine decay published online by the EPA (Wahman, 2016). This online simulation allows users to input initial conditions including free chlorine concentration, free ammonia concentration, pH, total alkalinity, water temperature, total organic carbon (TOC) concentration, TOC fast reactive fraction, and TOC slow reactive fraction. Users were also allowed to select the length of the simulation between 2 to 60 days. At each time step, the online model reports concentrations of total chlorine, monochloramine, dichloramine, trichloramine, free chlorine, and free ammonia. To represent chloramine decay due to autodecomposition only, the initial TOC concentration was set to zero.

Auto-Batch model

The batch model simulating chloramine decay due to autodecomposition was validated against experimental data points of monochloramine decay over time found in Huang's (2008) work in addition to being validated against the EPA website. The experimental data points were

collected for a variety of water temperatures, pHs, initial chlorine to nitrogen ratios, and carbonate buffer concentrations. Experimental data from two scenarios with varying temperatures, pHs, initial chlorine to nitrogen ratios, and carbonate buffer concentrations was used along with the chloramine decay simulation published online by the EPA to validate that the autodecomposition batch model performed well under various environmental conditions. The two sets of conditions that were used for testing are shown in Table 2.10.

Table 2.10. Sets of environmental conditions that the autodecomposition batch model was validated for.

	Temperature (°C)	pH	Total Alkalinity (M)	Free Ammonia (M)	Free Chlorine (M)	$(Cl_2/N)_0$
Scenario 1	25	8.31	0.004	1.00E-4	5.00E-5	0.5
Scenario 2	4	7.5	0.01	7.14E-5	5.00E-5	0.7

The autodecomposition batch model was validated for both sets of environmental conditions shown in Table 2.10. The results of the validation against experimental data and the results of the online chloramine decay simulation published by the EPA for the scenario 1 conditions are shown in Figure 2.4 and for the scenario 2 conditions are shown in Figure 2.5. The model performs well under both sets of conditions.

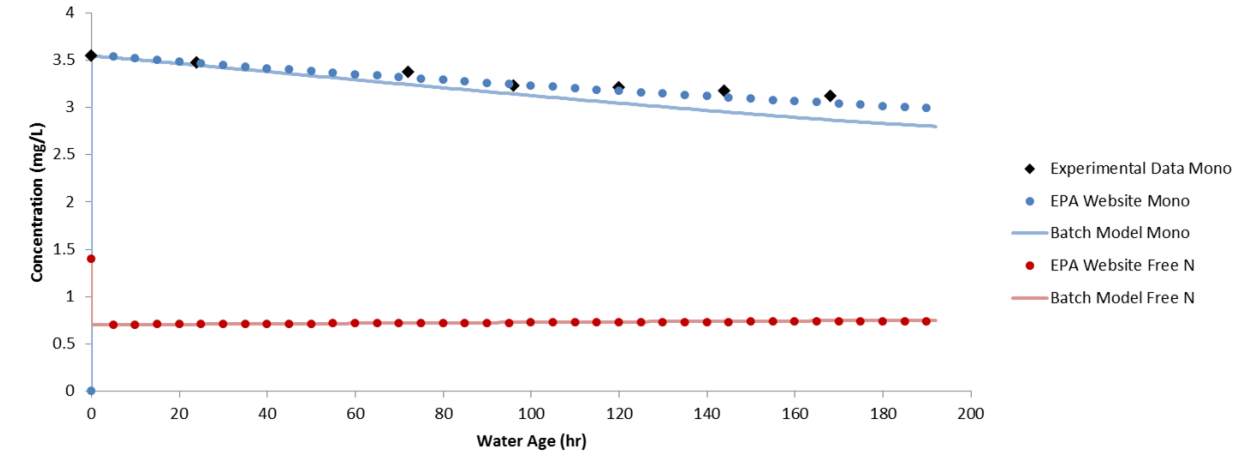

Figure 2.4. Validation of the autodecomposition batch model against outputs from the chloramine decay simulation published online by the EPA (Wahman, 2016) under the first set of environmental conditions (Scenario 1).

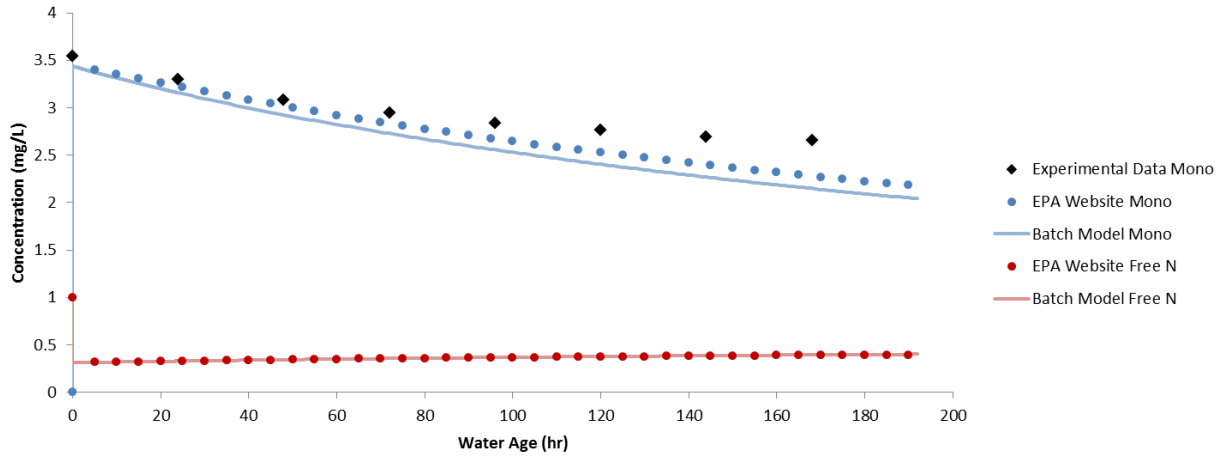

Figure 2.5. Validation of the autodecomposition batch model against outputs from the chloramine decay simulation published online by the EPA (Wahman, 2016) under the second set of environmental conditions (Scenario 2).

AutoDOC-Batch model

The batch model simulating chloramine decay due to autodecomposition and the presence of NOM was validated against the EPA website. No experimental data was available to validate this model against. The values that the EPA website used for k_{DOC1} and k_{DOC2} are not obvious. The website states that their simulation uses the average fast and slow organic reaction rate constants from Duirk et al. (2005), but when these average values were input into the AutoDOC-Batch model, the results do not match the website results. However, the EPA website results can be matched using k_{DOC1} and k_{DOC2} values that have been calibrated to the EPA website output using MATLABs lsqcurvefit function. The calibrated values of k_{DOC1} and k_{DOC2} fall outside the expected values for k_{DOC1} and k_{DOC2} reported in Duirk et al. (2005). The results of the validation using the calibrated parameter values are shown in Figure 2.6.

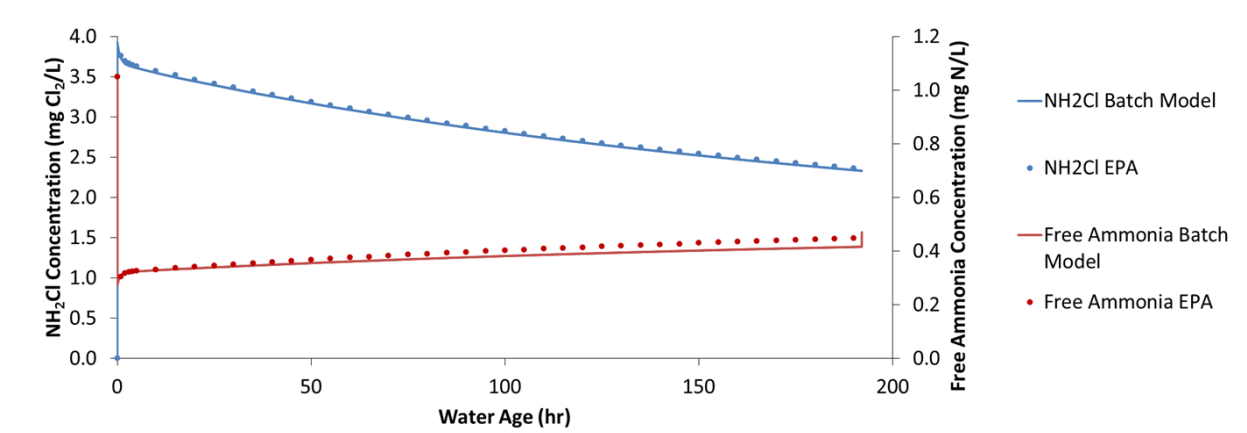

Figure 2.6. Validation of AutoDOC-Batch model against outputs from the chloramine decay simulation published online by the EPA (Wahman, 2016). Parameters that required calibration were k_{DOC1}, k_{DOC2}, S_1, and S_2. The calibrated parameter values were 3.45E4, 1.0E5, 0.016, and 0.57 respectively.

2.4.3 MSX Model Validation

Auto-MSX-Simple model

The EPANET-MSX model simulating chloramine decay due to autodecomposition was first tested with a simple hydraulic network consisting of a reservoir, five pipes, and four nodes, shown in Figure 2.7. A mass balance on chloramine was performed at each node using the pipe flows and node demands output by the EPANET hydraulic model and monochloramine concentrations at the nodes and pipes output by the EPANET-MSX water quality model, shown in Table 2.11. The mass balance was satisfied at each node, as shown in Table 2.12.

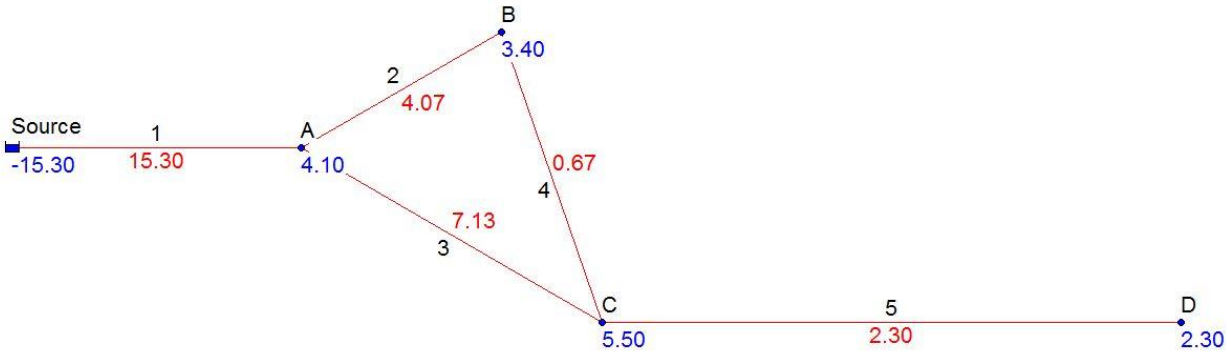

Figure 2.7. Simple hydraulic network with pipe flows in liter per minute (LPM) shown in red along pipes and node demands in LMP shown in blue next to nodes. Pipe and node names are shown in black text.

Table 2.11. Monochloramine concentrations output by EPANET-MSX at all nodes and pipes in the simple hydraulic network.

Node	NH_2Cl Concentration (mg/L)	Pipe	NH_2Cl Concentration (mg/L)
A	3.93	1	3.91
B	3.88	2	3.91
C	3.83	3	3.89
D	3.64	4	3.71
		5	3.73

Table 2.12. Monochloramine mass balance at each node of the simple hydraulic network. Pipe flows and node demands output by the EPANET hydraulic model and monochloramine concentrations at the nodes and pipes output by the EPANET-MSX water quality model were used for the mass balance. Slight discrepancies between mass in and mass out at nodes B and C are due to an inconsistency between node and pipe reporting that has been brought to the attention of the EPANET-MSX developers.

Node	Mass In (mg/min)	Mass Out (mg/min)
A	59.8	59.8
B	15.9	15.7
C	30.2	29.6

After verifying that the mass balance was satisfied, the monochloramine concentrations reported by EPANET-MSX were validated against results from an online chloramine decay model published by the EPA (Wahman, 2016) and the previously validated autodecomposition batch model using node water age. The results of the validation are shown in Figure 2.8.

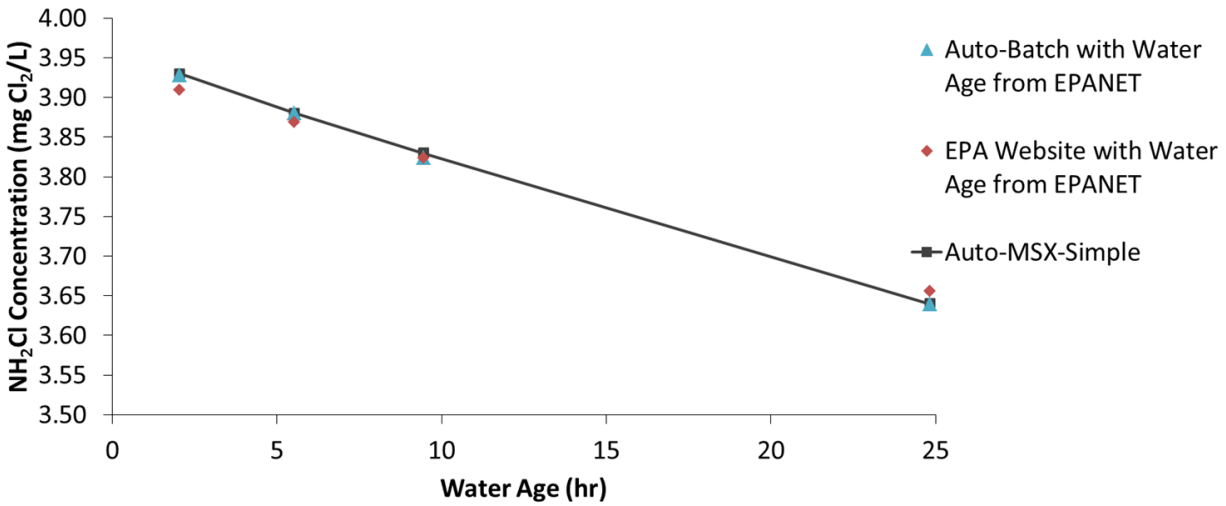

Figure 2.8. Results from the autodecomposition EPANET-MSX model applied to the simple hydraulic network validated against outputs from the chloramine decay simulation published online by the EPA (Wahman, 2016) and the previously validated autodecomposition batch model using water age.

Auto-MSX-Cary model

Once the EPANET-MSX model simulating chloramine decay due to autodecomposition was validated for the simple hydraulic network, it was applied to the calibrated hydraulic model of the Town of Cary's water distribution system. The hydraulic model was run with the EPANET-MSX autodecomposition model for seven days of simulation. Though the hydraulic model was developed for the entire month of August 2017, the MSX simulation was only run for seven days due to the extended run time required for a full month of simulation. The seven days simulated by the model correspond to the first week of August 2017. Total chlorine concentrations were reported at model nodes corresponding to locations where field samples were taken in the first week of August 2017. The concentrations reported by the model at the hour of simulation closest to the time at which the field sample was taken were compared to the measured total chlorine values. These model reported concentrations and the measured total chlorine concentrations are shown in Table 2.13. Since this model only accounts for chloramine decay due to autodecomposition and in real systems chloramine decays due to autodecomposition and

reactions with NOM, inorganics, and pipe walls, we expect the measured concentrations to be lower than the model concentrations. The concentrations output by the model represent a ceiling on total chlorine concentrations at each point, as autodecomposition always occurs. Additional decay reactions will further reduce chloramine concentrations, resulting in concentrations lower than the concentrations output by the autodecomposition model. This was confirmed as the model reported concentrations at 17 of the 19 sampling points shown in Figure 2.9 were higher than the measured concentrations.

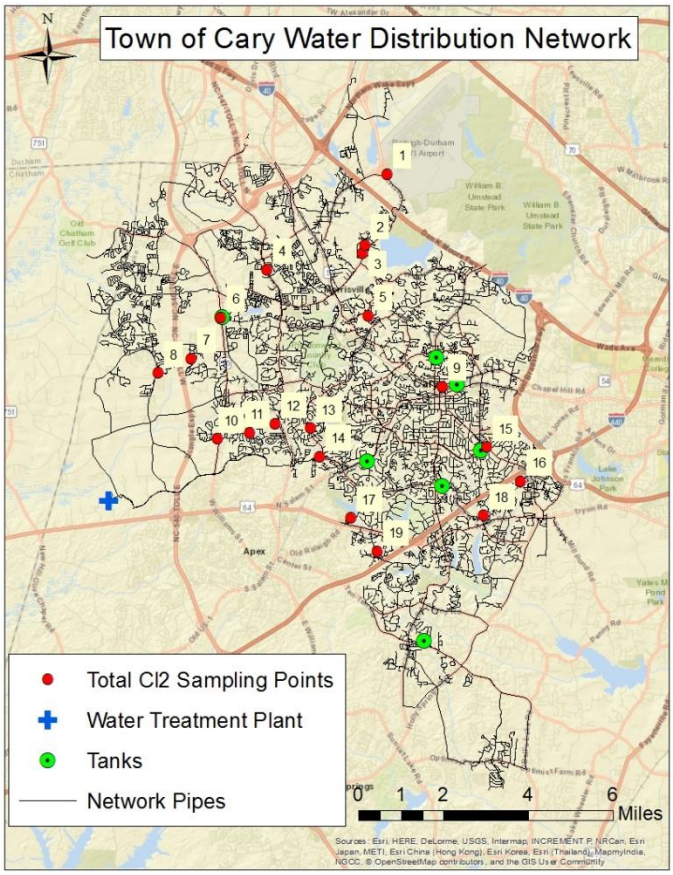

Figure 2.9. Points in the Cary water distribution network at which total chlorine samples were taken. Numbers at sampling points correspond to sample site in Table 2.13.

Table 2.13. Total Cl_2 concentrations measured at various points in Cary's water distribution network and model reported total Cl_2 concentrations at the same locations in the network. Model concentrations were taken from the hour of simulation corresponding to the hour at which the sample was taken in the field.

Sample Site	Total Cl_2 Measured (mg/L)	Total Cl_2 Model (mg/L)
1	3.12	3.57
2	3.40	3.57
3	2.95	3.68
4	2.89	3.07
5	2.75	3.81
6	2.93	3.18
7	2.89	3.66
8	3.32	3.11
9	3.41	3.53
10	3.61	3.88
11	3.44	3.80
12	3.68	3.82
13	3.65	3.81
14	3.67	3.75
15	3.05	2.92
16	2.41	2.88
17	3.21	3.67
18	2.83	2.83
19	3.42	3.55

AutoDOC-MSX-Simple and AutoDOC-MSX-Cary models

In our attempts to model chloramine decay due to autodecomposition and the presence of NOM using EPANET-MSX, we were unable to capture the biphasic nature of the decay. Chloramine concentrations should experience a sharp drop over the first few hours and then decay at a lesser rate, as shown in Figure 2.5. However, our attempts to model this with EPANET-MSX have not captured the initial sharp drop in concentration, resulting in the autodecomposition + DOC model reporting concentrations nearly identical to the autodecomposition model. The results of running the autodecomposition + DOC EPANET-MSX model with the simple hydraulic network are shown in Appendix B, along with the expected results output by the chloramine decay model published by the EPA and the autodecomposition + DOC batch reaction model. Because we

haven't been able to capture this initial fast decay, we were unable to use EPANET-MSX to model chloramine decay due to autodecomposition and the presence of NOM in the simple hydraulic network model or Cary's hydraulic network model.

2.4.4 Batch Model with Water Age from Hydraulic Model Validation

AutoDOC-Batch with water age from Cary EPANET

Since we are currently unable to model chloramine decay due to autodecomposition and the presence of NOM using EPANET-MSX, we used the validated batch model along with water age from the calibrated hydraulic model for August 2017 to predict chloramine concentrations throughout Cary's distribution network. To account for variations in daily demand and operation, hourly water age reported by the calibrated hydraulic model was averaged at each sampling node for the day of simulation corresponding to the day the sample was taken. This captures temporal variation in chloramine concentrations at a daily scale. The measured concentration at each sampling point was plotted against the average water age from the calibrated hydraulic model for the day of sampling in Figure 2.10.

To see if extracting water age from a calibrated hydraulic model built with hourly measured demands resulted in better prediction of total chlorine concentrations than extracting water age from a typical planning model built with average demand patterns, we plotted concentration at each sampling point as a function of water age from the planning hydraulic model in Figure 2.11. Hourly water age reported by the planning hydraulic model was averaged at each sampling node for the seventh day of simulation, after the model had reached steady state.

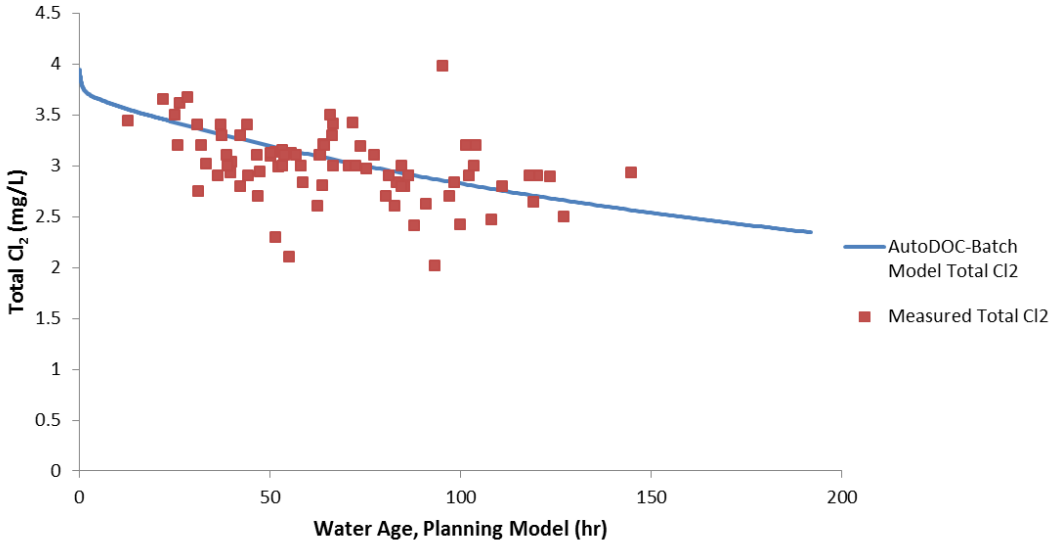

Figure 2.10. Total Cl_2 concentrations output by the AutoDOC-Batch model and measured total Cl_2 concentrations plotted as a function of water age. Water age for the field measurements was determined using the planning hydraulic model for Cary's distribution system.

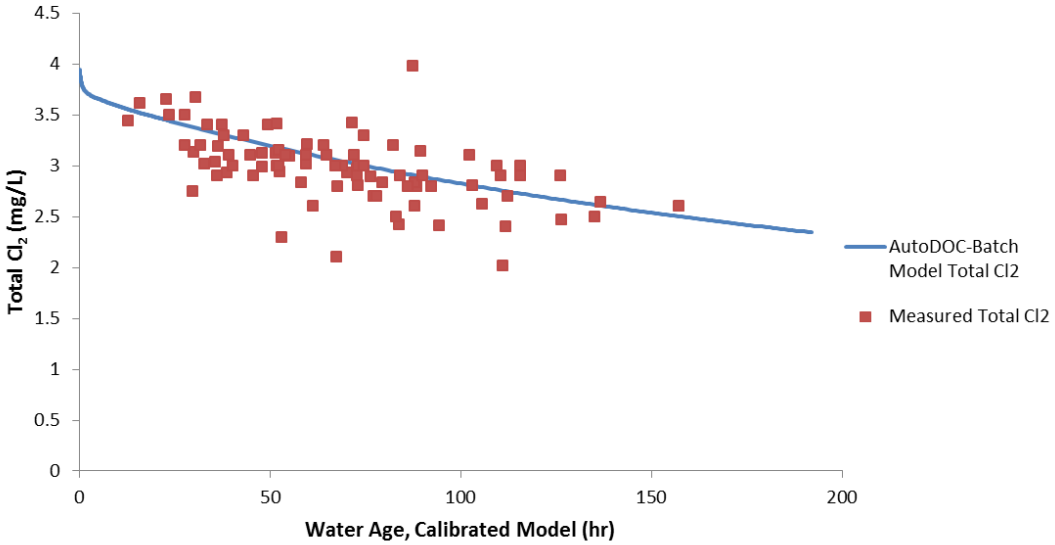

Figure 2.11. Total Cl_2 concentrations output by the AutoDOC-Batch model and measured total Cl_2 concentrations plotted as a function of water age. Water age for the field measurements was determined using the calibrated hydraulic model for Cary's distribution system.

The AutoDOC-Batch model predicts the measured total chlorine concentrations as a function of water age fairly well in both Figure 2.10 and Figure 2.11. However, the correlation coefficient

between the outputs of the batch reaction model and the measured points as a function of calibrated hydraulic model water age (R^2=0.33) is higher than the correlation coefficient between the outputs of the batch reaction model and the measured points as a function of planning hydraulic model water age (R^2=0.21). This shows that when using water age extracted from a hydraulic model in conjunction with a batch reaction model to predict total chlorine concentrations, using water ages from a calibrated hydraulic model built with measured hourly demands results in better predictions than using water ages from a typical planning hydraulic model.

The results shown in Figure 2.11 indicate that water ages from a well calibrated hydraulic model can be used in conjunction with the chloramine decay model presented in this work to predict chloramine concentrations spatially throughout a full scale distribution network. Chloramine concentrations can be predicted temporally on a daily scale to account for daily demand and operation variations as well.

2.5 Conclusions

In conclusion, we have applied a chloramine autodecomposition model for a batch reaction system and validated it under a range of environmental conditions reflective of conditions encountered in water distribution systems. We have also modeled chloramine decay due to autodecomposition and the presence of NOM for a batch reaction system and validated the model. The batch reaction model of chloramine decay due to autodecomposition and the presence of DOC can be used in conjunction with water age from a well calibrated hydraulic model to predict total chlorine concentrations spatially and temporally throughout a water distribution network. This was verified in a case study carried out to the Cary/Apex Water Treatment Facility and distribution system by comparing total chlorine samples taken at various

points in the network on different days to the total chlorine concentrations predicted by pairing hydraulic model water age with the autodecomposition + DOC batch model. We also showed that using water age extracted from a calibrated hydraulic model built with hourly measured demands in conjunction with a batch reaction model led to better predictions of total chlorine concentrations throughout the network than using water age extracted from a planning hydraulic model built with average demand patterns.

We also applied the chloramine autodecomposition and autodecomposition + DOC models with the EPANET-MSX toolkit in the hope that this would allow us to more accurately predict concentrations of disinfectants spatially and temporally. The autodecomposition MSX model was validated for a simple hydraulic network. The autodecomposition MSX model was then used with the calibrated hydraulic model of the Town of Cary's water distribution system built with hourly measured demands from August 2017. This autodecomposition model can be used to set an upper limit on expected concentrations throughout the network, as autodecomposition always occurs and additional decay reactions will further reduce chloramine concentrations, resulting in concentrations lower than the concentrations output by the autodecomposition model. This was confirmed as the model reported concentrations at 17 of the 19 selected sampling points were higher than the measured concentrations. However, the MSX model of chloramine autodecomposition in the presence of DOC results could not be verified for the simple or full scale hydraulic network since these models didn't capture the biphasic nature of the reaction. Future work involves identifying bugs and improving EPANET-MSX programming, which can then be used to model chloramine decay in a full scale system successfully in all conditions.

SUMMARY

This thesis focused on two aspects, one relating to operational hydraulics and the other relating to operational water quality, that were prepared as two papers, chapters 1 and 2 respectively. From the paper presented in chapter 1, it was concluded that:

- Reduction of model error can be achieved by the incorporation of data from pressure reducing valve (PRV) monitoring, operational monitoring, and supervisory control and data acquisition (SCADA) systems into network models.
- Incorporating PRV monitoring data only affects the model during hours that the PRV is open. Model improvement from PRV monitoring data increases as the PRV reaches steady state. Model improvement is seen in areas hydraulically near the PRV.
- Incorporating operational monitoring data only results in model improvement when paired with SCADA data.
- Incorporating SCADA data results in the most model improvement of the three data types.
- The most model improvement is achieved by incorporating all three data types together.

From the paper presented in chapter 2, it was concluded that:

- A batch reaction model of chloramine decay due to autodecomposition and the presence of DOC can be used in conjunction with water age from a well calibrated hydraulic model to predict total chlorine concentrations spatially and temporally throughout a water distribution network.
- Using water age extracted from a calibrated hydraulic model built with hourly measured demands led to better predictions of total chlorine concentrations throughout the network

than using water age extracted from a planning hydraulic model built with average demand patterns.

- An EPANET-MSX model of chloramine decay due to only autodecomposition can be used in conjunction with a calibrated hydraulic model to estimate an upper limit for total chlorine concentrations spatially and temporally throughout a distribution system.

REFERENCES

Bates, R.G., Pinching, G.D. (1949). Acidic dissociation constant of ammonium ion at 0º to 50º C, and the base strength of ammonia. Journal of Research of the National Bureau of Standards, 42, 419-430.

CH2M HILL (2009). Town of Cary Water Distribution System Master Plan.

Duirk, S.E., Gombert, B., Croue, J., Valentine, R.L. (2005). Modeling monochloramine loss in the presence of natural organic matter. Water Research, 39, 3418-3431.

Duirk, S.E., Valentine, R.L. (2007). Bromide oxidation and formation of dihaloacetic acids in chloraminated water. Environmental Science & Technology, 41(20), 7047-7053.

EPANET 2.0 [Computer software]. (2008). Retrieved from https://www.epa.gov/water-research/epanet

Granstrom, M.L. (1954). The disproportionation of monochloramine. Doctoral dissertation, Harvard University, Cambridge, MA.

Hand, V.C., Margerum, D.W. (1983). Kinetics and mechanisms of the decomposition of dichloramine in aqueous solution. Inorg. Chem., 22(10), 1449-1456.

Huang, X. (2008). Reactions between aqueous chlorine and ammonia: a predictive model. Doctoral dissertation, Northeastern University, Boston, MA.

H2ONET 15.0 [Computer software]. (2018). Retrieved from http://www.innovyze.com/products/h2onet/

Jafvert, C.T. (1985). A unified chlorine-ammonia speciation and fate model. Doctoral dissertation, University of Iowa, Iowa City, IA.

Jafvert, C.T., Valentine, R.L. (1987). Dichloramine decomposition in the presence of excess ammonia. Water Research, 21(8), 967-973.

Jafvert, C.T., Valentine, R.L. (1992). Reaction scheme for the chlorination of ammoniacal water. Environmental Science & Technology, 26(3), 577-586.

Kirmeyer, G.J., Martel, K., Thompson, G., Radder, L., Klement, W.,LeChevallier, M., Baribeau, H., Flores, A. (2004). Optimizing chloramine treatment. AWWA Research Foundation, Denver, CO.

Kumar, K., Shinness, R.W., Margerum, D.W. (1987). Kinetics and mechanisms of the base decomposition of nitrogen trichloride in aqueous solution. Inorg. Chem., 26(21), 3430-3434.

Leao, S.F. (1981). Kinetics of combined chlorine: reactions of substitution and redox. Doctoral dissertation, University of California, Berkeley, Berkeley, CA.

Light Detection and Ranging (LIDAR). (2015, January). Retrieved from https://lta.cr.usgs.gov/lidar_digitalelevation

Margerum, D.W., Gray, E.T., Huffman, R.P. (1978). Chlorination and the formation of N-chloro compounds in water treatment. In Organometals and Organometalloids, Occurrence and Fate in the Environment (Edited by Brinkman, F.E., Bellama, J.M.), American chemical society symposium series, 82(17), 278-291.

MATLAB [Computer software]. (2018). Retrieved from https://www.mathworks.com/products/matlab.html

Monteiro, L., Figueiredo, D., Dias, S., Freitas, R., Covas, D., Menaia, J., Coelho, S.T. (2014). Modeling of chlorine decay in drinking water supply systems using EPANET MSX. Procedia Engineering, 70, 1192-1200.

Morris, J.C. (1966). The acid ionization constant of HOCl from 5 to 35º. The Journal of Physical Chemistry, 70(12), 3798-3805.

Morris, J.C., Issac, R.A. (1981). A critical review of kinetic and thermodynamic constants for the aqueous chlorine-ammonia system. In Jolley, R.L. et al. Water Chlorination: Environmental Impact and Health Effects, Vol. 4, 49-62. Ann Arbor Science, Ann Arbor, MI.

Ohar, Z., Ostfeld, A. (2014). Optimal design and operation of booster chlorination stations layout in water distribution systems. Water Research, 58, 209-220.

Ozekin, K., Valentine, R.L., Vikesland, P.J. (1996). Modeling the decomposition of disinfecting residuals of chloramine. In Minear and Amy; Water Disinfection and Natural Organic Matter, 115-125. ACS Books, Washington, DC.

Sawade, E., Monis, P., Cook, D., Drikas, M. (2015). Is nitrification the only cause of microbiologically induced chloramine decay?. Water Research, 88, 904-911.

Shang, F., Uber, J.G., Rossman, L. (2008). EPANET Multi-species extension software and user's manual. U.S. Environmental Protection Agency, Washington, DC. EPA/600/C-10/002.

Siew, C., Tanyimboh, T., 2012. Pressure-dependent EPANET extension. Water Resources Management 26 (6), 1477-1498.

Snoeyink, V.L., Jenkins, D. (1980). Water Chemistry. New York, John Wiley & Sons, Inc.

USEPA (2010). Comprehensive disinfectants and disinfection byproducts rules (stage 1 and stage 2): quick reference guide. U.S. Environmental Protection Agency, Washington, DC.

Vikesland, P.J., Ozekin, K., Valentine, R.L. (2001). Monochloramine decay in model and distribution system waters. Water Research, 35(7), 1766-1776.

Wahman, D.G. (2016). Reactor simulation of drinking water chloramine formation and decay (version 0.52). U.S. Environmental Protection Agency, Office of Research and Development, Washington, DC. Retrieved from https://usepaord.shinyapps.io/Unified-Combo/

WaterCAD [Computer software]. (2017). Retrieved from https://www.bentley.com/en/products/product-line/hydraulics-and-hydrology-software/watercad

WaterGEMS [Computer software]. (2017). Retrieved from https://www.bentley.com/en/products/product-line/hydraulics-and-hydrology-software/watergems

Wilczak, A., Jacangelo, J.G., Marcinko, J.P., Odell, L.H., Kirmeyer, G.J., Wolfe, R.L. (1996). Occurrence of nitrification in chloraminated distribution systems. Journal – American Water Works Association, 88(7), 74-85.

Zhang, Y., Triantafyllidou, S., Edwards, M. (2008). Effect of nitrification and GAC filtration on copper and lead leaching in home plumbing systems. Journal of Environmental Engineering, 134(7), 521-530.

Zhu, X., Zhang, X. (2016). Modeling the formation of TOCl, TOBr and TOI during chlor(am)ination of drinking water. Water Research, 96, 166-176.

APPENDICES

Appendix A

August 2017 tank levels measured with SCADA compared to tank levels from the calibrated hydraulic model for the Field Street Tank (top), Maynard Tank (second down), Old Apex Tank (third down), and Ridgeview Tank (bottom).

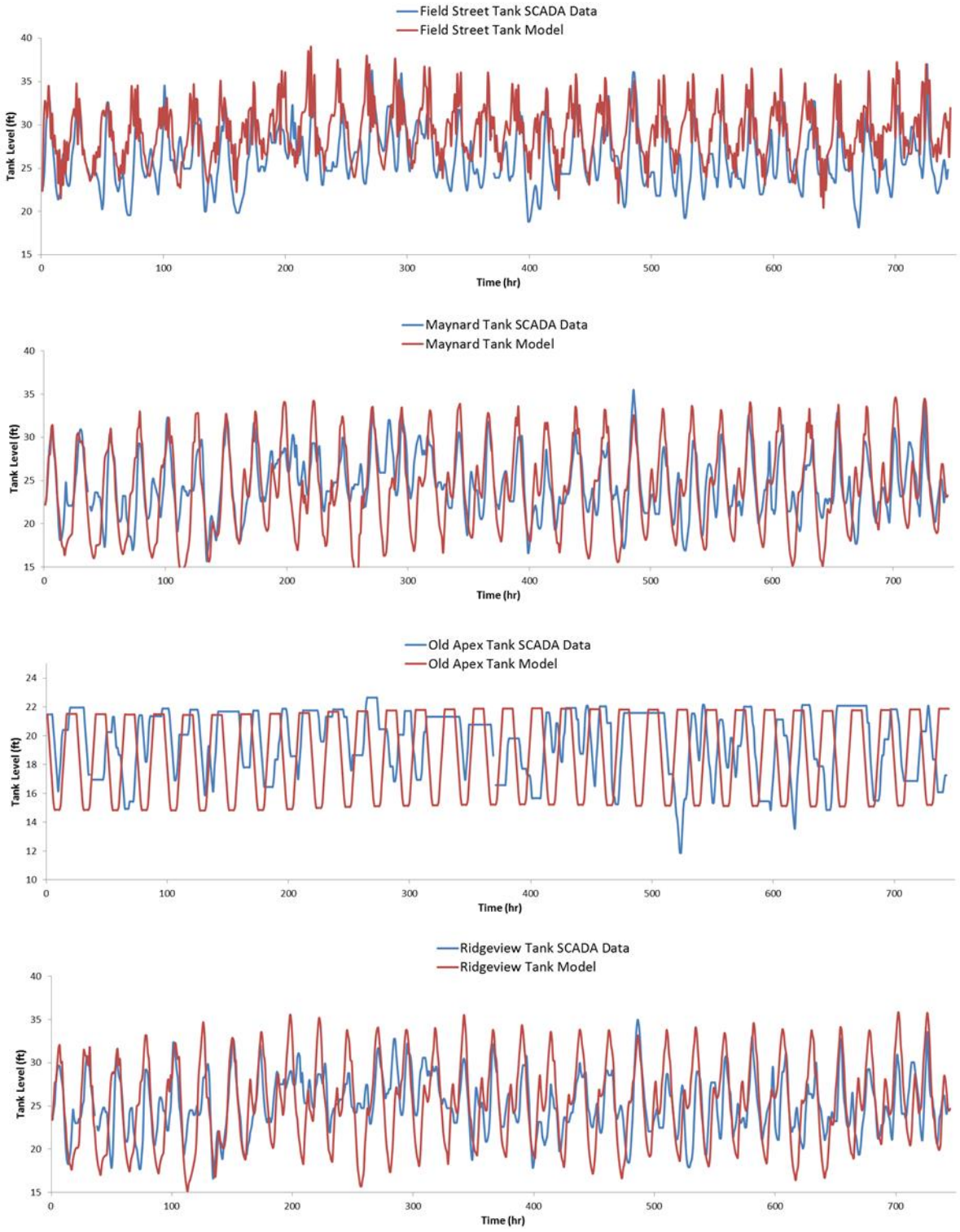

Appendix B

Results from the autodecomposition + DOC EPANET-MSX model applied to the simple hydraulic network plotted against outputs from the chloramine decay simulation published online by the EPA (Wahman, 2016) and the previously validated autodecomposition + DOC batch model using water age.